Surface modification and bonding of advanced polymer materials through vacuum ultraviolet (VUV) -induced technology

真空紫外線を用いた先端機能性高分子材料の表面改質と接合

Weixin   FU

付   偉欣

February, 2018

Surface modification and bonding of advanced polymer materials through vacuum ultraviolet (VUV) -induced technology

真空紫外線を用いた先端機能性高分子材料の表面改質と接合

Weixin   FU

付   偉欣

Waseda University
Graduate School of Advanced Science and Engineering
Department of Nanoscience and Nanoengineering
Research on Nano and Microsystems

February, 2018

Doctoral dissertation committee:

Professor
Dr. Shuichi Shoji (supervisor)
Faculty of Science and Engineering
Waseda University

Professor
Dr. Hiroshi Kawarada
Faculty of Science and Engineering
Waseda University

Professor
Dr. Takanobu Watanabe
Faculty of Science and Engineering
Waseda University

Principal Researcher
Dr. Akitsu Shigetou
Research Center for Structural Materials
National Institute for Materials Science

Professor
Dr. Jun Mizuno
Research Organization for Nano and Life
Innovation
Waseda University

Acknowledgement

This thesis describes a direct atmospheric low temperature hybrid bonding technology realized by surface modification methods for both advanced polymer materials and metals.   The proposed methods are expected to be utilized as polymer-metal hybrid packaging technology in future implantable biomedical applications.   There are many contributors and collaborators in this work.

First, I sincerely thank my supervisor, Professor Shuichi Shoji at faculty of Science and Engineering of Waseda University, for giving me the opportunity to study and research in such a nice environment. Without his supports and advices, this work cannot have been accomplished.

I want to deeply thank the dissertation committee, Professor Hiroshi Kawarada and Professor Takanobu Watanabe at Faculty of Science and Engineering of Waseda University, and Principal Researcher Akitsu Shigetou at National Institute for Materials Science, for their careful reading and fruitful discussions.   Especially, I appreciate Principal Researcher Akitsu Shigetou again for her encompassing supports during my doctoral enrollment, which greatly helped me.

I sincerely appreciate Professor Jun Mizuno at Nanotechnology Research Center of Waseda University, for his constructive technical advices and warm support.   He has kindly supported me for over 5 years since I started as a student researcher in graduate school.

I am grateful to Professor Tetsushi Sekiguchi, Professor Mikiko Saito and Associate Professor Isamu Yuito at Nanotechnology Research Center of Waseda University for their kind advices that associated my Ph.D. studies.

I also want to give my thanks to students in Shoji laboratory, especially the members in GIT groups: Mr. Hiroyuki Kuwae, Mr. Hirokazu Noma, Mr. Bingyang Xu, Mr. Atsuki Nobori, Ms. Haruka Suzaki, Mr. Seren Maeda, Mr. Takumi Kamibayashi, Mr. Kosuke Sakamoto, Mr. Kenichi Atsumi, Ms. Mayuko

Shiozawa, Mr. Keito Miwa, Mr. Kosuke Yamada, Ms. Akiko Fujiwara, and Ms. Akari Otsuka, for their supporting in my daily research lives. Mr. Daiki Tanaka is my contemporary Ph.D. student in Shoji laboratory, whom I am happy to complete doctorate together with. I would also like to give great thanks to Ms. Reiko Nishikiori for her kind support of official procedure.

I would also like to thank the Nanotechnology Support Project of Waseda University and the Leading Graduate Program in Science and Engineering of Waseda University from MEXT for their help.

Finally, I give my faithful appreciation to my family, my parents and grandparents, for allowing my enrollment at the Ph.D. course, as well as their financially supports and continuous encouragement. Without their support, I could never make it so far. At last, I would like to express my thanks to Peiying Sun. Her grace and kindness enlighten my future life.

I sincerely appreciate again to everyone with me.

Weixin FU

Table of Contents

List of figures

List of tables

List of abbreviations

AFM: atomic force microscope

APTES: (3-aminopropyl)triethoxysilane

Bio-MEMS: biomedical micro electromechanical system

FAB: fast atom beam bombardment

GOPTS: (3-glycidyloxypropyl)trimethoxysilane

LMWOM: low molecular weight oxide material

MEMS: micro electromechanical system

MMA: methyl methacrylate

PEEK: poly ether ether ketone

PMMA: polymethyl methacrylate

POM: polyoxymethylene

VUV: vacuum ultraviolet

SAM: self-assembled monolayer

SEM: scanning electron microscope

SPAR: surface pore area ratio

TBB: partly oxidized tri-n-butyl boron

XPS: x-ray photoelectron spectroscopy

4-META: 4-methacryloyloxyethy trimellitate anhydride

Chapter 1

Introduction

1.1　Background and Motivation

　　Hybrid integration of diverse materials is an essential breakthrough to multiple technological fields because we can achieve reciprocating materials properties, such as hardness and toughness, at the same time.　Particularly, the hetero integration of metals and polymers is highly attractive to the fields of bio-medical electronic packaging and lightweight structural material due to its flexibility and low fabrication cost, which may contribute in realizing a lightweight and "smart" material for Internet on Things (IoT). However, because the human safety will be one of the key issues to such IoT hybrid materials, conventional hybridization methods like adhesives are becoming difficult to be utilized due to their comparably low interfacial reliability.　A direct, robust, non-toxic, and easy-to-use assembly, i.e. bonding, method is highly required to polymers and metals.

　　For this, a compatible bondability should be created simultaneously to the diverse materials at low temperature.　In addition, the bonding process has to be carried out without vacuum atmosphere for the sake of productivity in actual industry.　Therefore, we have proposed a novel bonding method utilizing vacuum ultraviolet (VUV) surface modification, which is supported by the formation of ultrathin compatible bridge layers.　In this thesis, the underlying technologies such as the evolution of chemical binding status, bond formation mechanism, bond strength and so on are elaborated on.　Furthermore, some examples of hybrid bonding are demonstrated using typical engineering polymers and metals.

1.1.1. Hybrid integration between polymers and metals

Table 1.1 List of advanced polymer materials [12]

Acronym	Full name	Temperature stability [°C]	Properties	Structure
COC	Cyclo-olefine copolymer	140	High transparency	Amorphous
PMMA	Polymethylmethacrylate	80	High transparency	Amorphous
PC	Polycarbonate	130	High transparency	Amorphous
PS	Polystyrene	80	Transparent	Amorphous
POM	Polyoxymethylene	90	Low friction	Semi crystalline
PFA	Perfluoralkoxy copolymer	260	High chemical resistivity	Semi crystalline
PVC	Polyvinlchloride	60	Cheap	Amorphous
PP	Polypropylene	110	Mechanical properties	Semi crystalline
PET	Polyethylene terephtalate	110	Transparent, low friction	Amorphous/Semi crystalline
PEEK	Polyetheretherketone	250	High temperature resistivity	Semi crystalline
PA	Polyamide	80–120	Good mechanical properties	Semi crystalline
PSU	Polysulfone	150	Chemical and temperature resistivity	Amorphous
PVDF	Polyvinylidenefluoride	150	Chemically inert, piezo-electric	Semi crystalline

Biomedical micro electromechanical system (bio-MEMS) attracted increasing attentions for future health monitoring and therapy methods [1-8] in the past few decades because of its advantages such as miniaturization, lightweight, low power consumption and high reliability [9]. Especially, implantable bio-MEMS became attractive because it could provide continuous monitoring and long-term curing [10, 11]. The implant bio-MEMS required flexibility in shape and chemical tolerance for sake of compatibility to internal body movement. Consequently, it was quite predictable that we needed to replace conventional brittle packaging materials with flexible polymer materials (**Table 1.1** [12]). Those polymer materials were widely chosen to bio-MEMS applications because of high robustness against critical environment inside the body such as moisture, acid, and so on. Among these promising materials, we select poly-oxymethylene (POM) and poly-etheretherketone (PEEK) (**Fig. 1.1**) as the starting materials for hybridization, because they have high toughness and mechanical strength, tolerance to chemical solvents and radioactive, good dielectricity [13-28]. Additionally, these engineering materials are available at low production cost and already adopted to the field of structural materials. From the viewpoint of bio-MEMS devices, it was inevitable that the insulation polymer substrates had to be hybridized with wiring metals in order to secure the electronic interconnection between the sensing source and control chip (**Fig. 1.2**). However, a bottom-up direct fabrication, such as photolithography, was highly difficult to the combination of organic/inorganic materials due to the differences in production scheme and bond mechanisms inside the materials. Therefore, a discrete assembly (i.e. bonding) was
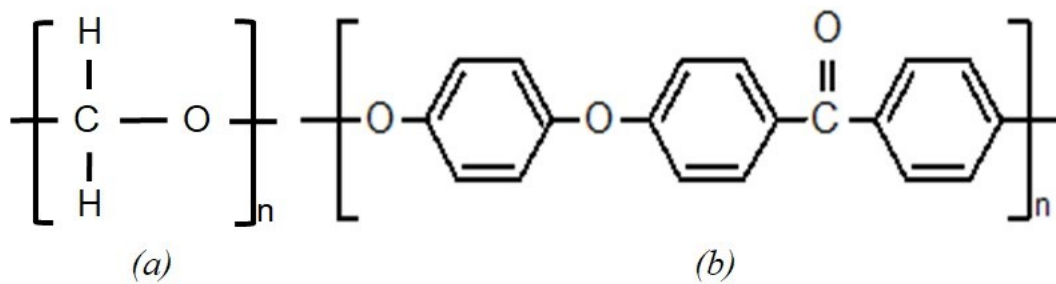
Fig. 1.1 Chemical structural formula of (a) POM and (b) PEEK
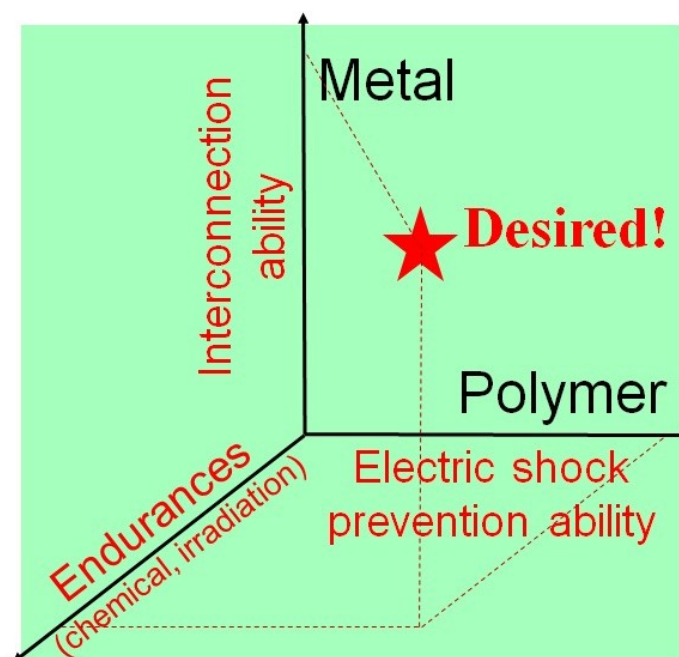
Fig. 1.2 Breakthrough physical limit of homogenous material: obtaining electro-conductivity and electric shock prevention ability simultaneously by metal-polymer hybrid

inevitable to the integration of polymers and metals.

In order to create sufficient bondability among polymers and metals, there were three kinds of interfaces we had to create at the same time, which were between polymer-polymer, metal-metal, and polymer-metal (**Fig. 1.3**). This was because a thick adhesion layer such as solder ball should be eliminated to maintain the interfacial flexibility so that the thermal strain could be compensated by deforming whole body. Consequently, all the materials were supposed to appear on the same plane to
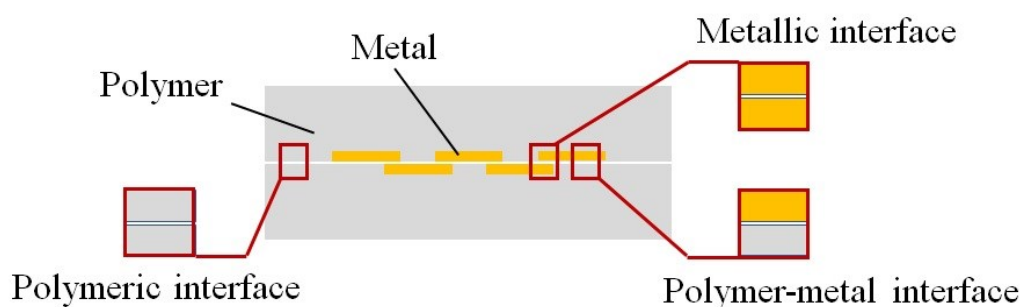
Fig. 1.3 Schematic image of three interfaces in polymer-metal hybrid: a polymeric interface, a metallic interface and a polymer-metal interface.   These three interfaces require different bond mechanisms.

be bonded at the same time.   Here, the necessity of compatible bondability to diverse materials was generated.

In order to provide sufficient bondability to those diverse materials, we had to overcome some issues: (1) Low process temperature below glass transition temperature (T_g); (2) less matrix damage to organic materials to keep the materials properties; and (3) non-vacuum atmosphere for the compatibility to conventional industrial production.

1.1.2. Conventional bonding methods

1.1.2.1. Conventional polymer-metal bonding methods

Conventional polymer-metal bonding technologies included welding [29, 30], adhesives [29, 31-33] and mechanical fastening [29] (Table 1.2).   Welding method was the most consolidated method in many industry areas including polymers.   However, a direct welding between metal and polymer was not possible due to temperature that was too high to organic materials [29].   In addition, the polymer-metal welding was currently based on covering the metal component with polymer film and welding with another polymer component [29].   Such covering process required severe surface modifications using comparably high temperatures and chemical solvents, resulting in increasing turn-around-time (TAT). Furthermore, high temperature degraded the alignment accuracy due to the thermal expansion mismatch

4

Table 1.2 Conventional polymer-metal bonding technologies and their challenges

Methods	Challenges	Requirements
Welding	Heat damage Complex process	Low temperature Direct bonding (without adhesive) Atmospheric pressure process
Adhesive	Bio-toxicity High vacuum process	
Mechanical fastening	Not well sealed Stress concentration	

between diverse materials, thus ultrafine interconnection would be difficult for MEMS packaging. Adhesive bonding was a very effective method for diverse materials, but it may not be suitable in bio-MEMS because most adhesives risks of bio toxicity and low mechanical and thermal reliability. Some beam-induced surface modification techniques enabled the direct bonding between polymers and metals, however, most of those techniques required high vacuum conditions to accelerate high energy beam [33]. Also, those methods had a limitation in possible internal bond mechanisms. Another way to polymer-metal hybrid bond was mechanical fastening which had a straightforward process and provided extremely good bond strength. Nevertheless, this process tended to cause a stress concentration at highly-distorted interfaces in the scale of several tens micrometers, which was not suitable for bio-MEMS packaging.

1.1.2.2. Vacuum ultraviolet (VUV) treatment

Recently, the VUV technology was confirmed to be a suitable surface modification for polymer bonding [34, 35]. Because of the high photon energy of VUV, many kinds of chemical species could be dissociated, which often resulted in the elimination of surface contamination and/or replacement of outmost functional groups (i.e. the surface modification) [36]. Generally, the modification of surface was obtained via low molecular weight oxide material (LMWOM) formed on the outmost surface [34,

Table 1.3 Chemical bond energy and required dissociation wavelength

Chemical bond	Bond energy		Wavelength (nm)
	kcal/mol	kJ/mol	
C≡C	188.8	791.1	151
C≡N	222.2	931.0	129
C=O	190.0	796.1	151
C=C	140.5	588.7	204
H−F	134.9	565.2	212
O=O	117.5	492.3	243
C−F	115.2	482.7	248
O−H	109.3	458.0	262
H−Cl	101.9	427.0	281
C−H	97.6	408.9	293
N−H	91.9	385.1	311
C−C	84.3	353.2	339
C−Cl	76.9	322.2	372
C−O	76.4	320.1	374
C−N	63.6	266.5	450

35, 37-41].   Because the glass transition temperature of LMWOM layer was lower than that of the original polymers, the bonding could be achieved at low temperature almost directly in atmospheric pressure [34, 35, 37-41].   The values of chemical bond energy and corresponding required wavelength are exampled in **Table 1.3**.   Since (1) the possible candidates of functional groups to create bridging function were considered to be C-O and C-C in POM and PEEK, and (2) nitrogen atmosphere could be utilized as inert atmosphere during the VUV irradiation, we selected to use the light source with the wavelength of 172 nm.   However, once the combination of bonding included metals, a bondability cannot be obtained only by the VUV irradiation because thick and chemically stable surface compounds like oxide would not be dissociated by those energies.   Hence, a further activation source had to be involved in the VUV irradiation so that the bridging molecules could react with the surface and created covalent and/or coordinate bonds between polymers and metals.

1.2   **Proposal of new bonding method**

In order to achieve covalent/coordinate bonds between organic materials and metals at low temperature and atmospheric pressure, we proposed to utilize ultrathin aqueous compounds like metal hydrate as one of the most primitive and easiest-to-use materials for a bridge layer, because it could result from hydroxyl groups, carboxyl groups, amine groups and epoxy groups at low temperature.

However, given POM and PEEK as the starting materials, the bridge layer formation processes should be different according to the diverse operating temperature of those materials.   The operating temperature of POM was 110 ~ 120 °C, consequently the bonding must be realized at temperature lower than this, that was, the dehydration reaction cannot be adopted to POM.   Therefore, we selected to use another bridge formation method.   Because the surface of POM was easy to create amine and epoxy groups, which allowed to create chemical bonds between the surfaces at a temperature of 100 °C [42], we adopted self-assembled monolayer (SAM) including these groups after the VUV treatment.

On the other hand, in case of hybrid bonding between PEEK and other metal materials, which was tolerant of the process temperature higher than 250 °C, we could use the dehydration condensation reaction between the bridge layers, which would result in high bond strength, provided that the metal oxide was sufficiently deoxidized.   For this purpose, we proposed a vapor-assisted VUV technology (**Fig. 1.4**).
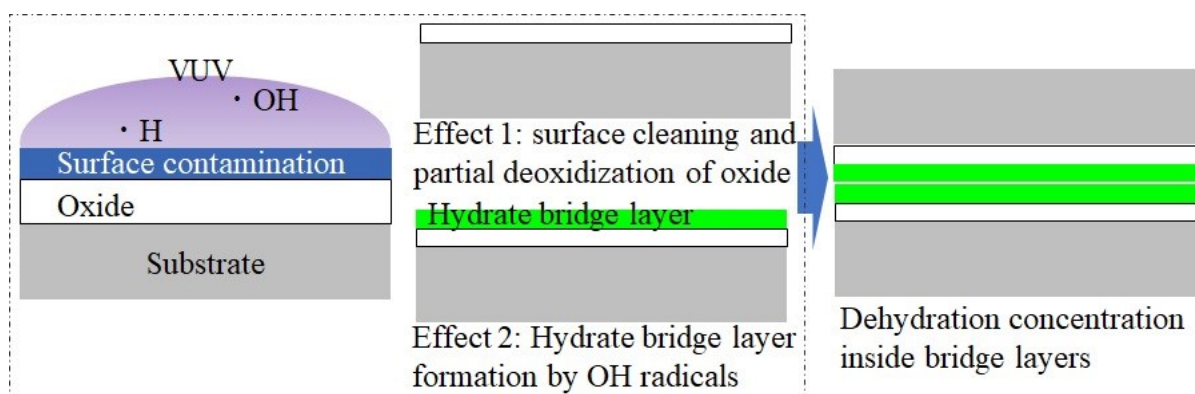
Fig. 1.4 Mechanism of the proposed vapor-assisted VUV modification on metal substrate

By introducing water vapor into the VUV irradiation as atmosphere at highly tuned humidity (i.e. the concentration of water molecules), hydrogen and hydroxyl radicals could be created through dissociating water molecules. These hydrogen radicals could partly deoxidize the surface of metal oxide to form sufficient cation sites, which further reacted with the hydroxyl radicals to create a hydrate bridge layer. As for PEEK surface, the hydroxyl radicals contributed in replacing the side chains to hydrophilic functional groups.

1.3 **Outline of thesis**

In order to realize these hybrid bonding technologies based on SAM and vapor-assisted VUV methods, the following issues are studied in this thesis:

(a) Evolution of surface chemical structures via surface modification,

(b) Optimization of process parameters,

(c) Bonding experiments and interfacial observations of nanostructures.

This doctoral thesis is consisted of six chapters: the synopses of other chapters are shown as follows:

Chapter 2 "**POM low temperature direct bonding**" describes POM surface modification methods by SAM. With these methods, direct bonding for POM substrates at 100 °C was achieved in atmosphere. Theoretical calculation was carried out to evaluate the bonding interface.

In Chapter 3 "**POM-PMMA room temperature bonding**", bonding between poly-methyl methacrylate (PMMA) and POM is proposed. The bonding was achieved at room temperature by using simple embedding process.

In Chapter 4 "**Vapor-assisted VUV surface modification technology**", a novel vapor-assisted VUV surface modification method was proposed. The proposed vapor-assisted VUV was capable of both polymer and metal surface modifications. An optimized condition for polymer modification was obtained through theoretical calculations and experimental study.

Chapter 5 "**PEEK-Pt low temperature direct bonding**" presents hybrid bonding of PEEK and Pt

through three different surface modification methods: vapor-assisted VUV, fast atom beam bombardment

and simple VUV.   Theoretical calculations were also carried out to evaluate the bonding interfaces.

Chapter 6 concludes this thesis and describes future research.

References

[1] Z. Li, E. Ye, David, R. Lakshminarayanan, X. J. Loh, Small, 12 (2016) 4782.

[2] X. J. Loh, T. Lee, Q. Doua, G. R. Deene, Biomater. Sci., 4 (2016) 70.

[3] Q. Dou, X. Fang, S. Jiang, P. L. Chee, T. Leed, X. J. Loh, RSC Adv., 5 (2015) 46817.

[4] K. Huang, Q. Dou, X. J. Loh, RSC Adv., 6 (2016) 60896.

[5] Q. Dou, C. P. Teng, E. Ye, X. J. Loh,, Int. J. Nanomedicine, 10 (2015) 419.

[6] E. Ye, X. J. Loh, Aust. J. Chem., 66 (2013) 997.

[7] C. Dhand, N. Dwivedi, X. J. Loh, A. N. J. Ying, N. K. Verma, R. W. Beuerman, R. Lakshminarayanan, S. Ramakrishna, RSC Adv., 5 (2015) 105003.

[8] B. M. Teo, D. J. Young, X. J. Loh, Part. Part. Syst. Charact., 33 (2016) 709.

[9] R. A. M. Receveur, F. W. Lindemans, N. F. J. De Rooij, Micromech. Microeng., 17 (2007) R50.

[10] D. H. Kim, J. Viventi, J. J. Amsden, J. Xiao, L. Vigeland, Y. S. Kim, J. A. Blanco, B. Panilaitis, E. S. Frechette, D. Contreras, Nat. Mater., 9 (2010) 511.

[11] R. Lo, P. Li, S. Saati, R. N. Agrawal, M. S. Humayun, E. Meng, Biomed. Microdevices, 11 (2009) 959.

[12] M. Heckele, W. K. Schomburg,, J. Micromech. Microeng., 14 (2004) R1.

[13] S. E. Sloop, M. M. Lerner, J. Electrochem. Soc., 143 (1996) 1292.

[14] Y. Dan-Mallam, M. Z. Abdullah, P. S. M. M. Yusoff, Polym. Compos.,35 (2014) 1900.

[15] C. Jama, O. Dessaux, P. Goudmand, L. Gengembre, J. Grimblot, Surf.Interface Anal., 18 (1992) 751.

[16] C. Y. Huang, C. I. Tseng, J. Appl. Polym. Sci., 78 (2000) 800.

[17] S. W. Ha, M. Kirch, F. Birchler, K. L. Eckert, J. Mayer, E. Wintermantel, C. Sittig, I. Pfund-Klingenfuss, M. Textor, N. D. Spencer, M. Guecheva, H. Vonmont, J. Mater. Sci.: Mater. Med., 8 (1997) 683 .

[18] S. Goossens, G. Groeninckx, Macromolecules, 39 (2006) 8049.

[19] S. Goossens, B. Goderis, G. Groeninckx, Macromolecules, 39 (2006) 2953.

[20] M. Aravand, S. V. Lomov, L. Gorbatikh, Compos. Sci. Technol., 110 (2015) 8.

[21] E. Kraus, L. Orf, B. Baudrit, P. Heidemeyer, M. Bastian, R. Bonenberger, I. Starostina, O. Stoyanov, Appl. Surf. Sci. 371 (2016) 365.

[22] P. Oyar, G. Can, Cumhuriyet Dent. J., 17 (2014) 205.

[23] S. M. Kurtz, J. N. Devine, Biomater., 28 (2007) 4845.

[24] J. F. Mano, R. A. Sousa, L. F. Boesel, N. M. Neves, R. L. Reis, Compos. Sci. Technol., 64 (2004) 789.

[25] D. H. Kim, J. Viventi, J. J. Amsden, J. Xiao, L. Vigeland, Y. Kim, J. A. Blanco, B. Panilaitis, E. S. Frechette, D. Contreras, D. L. Kaplan, F. G. Omenetto, Y. Huang, K. Hwang, M. R. Zakin, B. Litt, J. A. Rogers, Nat. Mater., 9 (2010) 511.

[26] D. Shukla, Y. S. Negi, J. S. Uppadhyaya, V. Kumar, Polym. Rev. 52 (2) (2012) 189–228.

[27] Y. Qin, M. M.R. Howlader, M. J. Deen, Y. M. Haddara, P. R. Selvaganapathy Sensors Actuators B Chem. 202 (2014) 758–778.

[28] T. Sasuga, M. Hagiwara, Polymer 27 (1986) 821–826.

[29] S. T. Amancio-Filho, J. F. dos Santos, Polym. Eng. Sci., 49 (2009) 1461.

[30] P. Mitschang, R. Velthuis, M. Didi, Adv. Eng. Mater., 15 (2013) 804.

[31] P. Molitor, V. Barron, T. Young, Int. J. Adhes. Adhes., 21 (2001) 129.

[32] P. Laurens, B. Sadras, F. Decobert, Arefi-Khonsari, J. Amouroux, Int. J. Adhes. Adhes., 18 (1998) 19.

[33] J. Comyn, L. Mascia, G. Xiao, B. M. Parker, Int. J. Adhes. Adhes. 16 (1996) 97–104.

[34] H. Shinohara, T. Kasahara, S. Shoji, J. Mizuno, J. Micromech. Microeng., 21 (2011) 085028.

[35] H. Shinohara, J. Mizuno, S. Shoji, Sens. Actuators A, 165 (2011) 124.

[36] W. Fu, B. Ma, H. Kuwae, S. Shoji, J. Mizuno, Jpn. J. Appl. Phys., 57 (2018) 02BB01.

[37] M. R. Davidson, S. A. Mitchell, R. H. Bradley, Surf. Sci., 581 (2005) 169.

[38] F. A. Rasoul, D. J. T. Hill, J. S. Forsythe, J. H. O'Donnell, G. A. George, P. J. Pomery, P. R. Young, J. W. Connell, J. Appl. Polym. Sci., 58 (1995) 1857.

[39] F. Truica-Marasescu, M. R. Wertheimer, Macromol. Chem. Phys., 206 (2005) 744.

[40] Y. Kim, Y. Taniguchi, K. Murase, Y. Taguchi, H. Sugimura, Appl. Surf. Sci., 255 (2009) 3648.

[41] R. M. Mahfouz, M. Sauer, S. T. Atwa, R. I. Kaiser, K. Roessler, Nucl. Instrum. Methods Phys. Res., Sect. B, 65 (1992) 447.

[42] M. Pramanik, E. W. Fowler, J. W. Rawlins, J. Coatings Technol. Res., 11 (2014) 143.

Chapter 2

POM low temperature direct bonding

This chapter elaborates a direct bonding of POM at low temperature of 100 °C via SAM.   Direct bonding for POM was a critical issue because POM had low surface free energy, and the bonding temperature could not be higher than 110 °C for sake of the low operating temperature.   To achieve such low temperature bonding, SAM was introduced to modify POM surfaces with amine- and epoxy-terminated molecules.   In order to adsorb SAMs on POM, VUV/O$_3$ treatment was carried out to create hydroxyl groups on POM surface, which further reacted with SAMs.   The modification effects were analyzed by XPS and SEM.   The XPS analysis showed that both amine- and epoxy-terminated SAMs adsorptions were successful.   Shear test showed the modification improved bonding strength.   The XPS also confirmed that VUV/O$_3$ treatment was effective on organic contamination removal and the subsequent POM C-O binding dissociation.   Since the excessive VUV/O$_3$ treatment would lead to POM surface degradation, an optimized process condition was obtained at 60 s process time.   The optimized bonding reached a strain release energy of 51.3 mN/m, which was at same level with POM surface free energy, and thus the bonding was strong enough.

2.1 **Introduction**

In Chapter 2, a direct low temperature poly-oxymethylene (POM) bonding technology was proposed. The bonding was achieved by surface modification, of which the effect was investigated.

As described in Chapter 1, in order to realize the low temperature POM bonding, it was necessary to create functional groups on POM surfaces. Thus, self-assembled monolayer (SAM) modification was introduced in POM bonding as that Tang and Lee reported room temperature bonding through amine- and epoxy-terminated SAMs in 2010 [1]. To achieve SAM adsorption, sufficient reactive group had to be created on POM in advance. Hence, surface activation using vacuum ultraviolet in presence of oxygen (VUV/O_3), which could dissociate POM C-O chain and create active dangling bonds, was required [2]. When water molecule approached on these active sites, the dangling bonds could react and form hydroxyl groups, which would further react with methyl groups in SAMs. On the other hand, a challenge could be predicted in this modification that the excessive VUV dissociation may cause surface degradation on POM. Therefore, the VUV/O_3 process dose must be optimized to balance activation and degradation.

In this section, POM surfaces were designed to be modified with amine- and epoxy-terminated SAMs. The modification was varied by the VUV/O_3 process time and the effect was investigated by surface morphology and bonding strength.
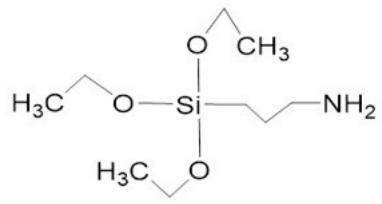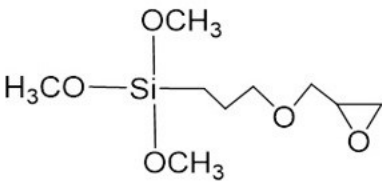
2.2 **POM surface modification and analyses**

2.2.1. Materials preparation

In this thesis, POM substrates were prepared at dimension of 20×10 mm with a thickness of 2 mm. Organic cleaning was carried out before surface modification following a standard chemical procedure: (1) Ethanol cleaning in ultrasonic bath for 5 min.

Table 2.1 Chemical formulas and functional groups of APTES and GOPTS

Solution	Chemical formula	Functional group
APTES		Amine
GOPTS		Epoxy

(2) Pure water cleaning in ultrasonic bath for no less than 5 min.

(3) Drying by a N_2 gun.

Applied SAMs were (3-aminopropyl)triethoxysilane (APTES) and (3-glycidyloxypropyl)trimethoxysilane (GOPTS). Their chemical formulas and functional groups were summarized in **Table 2.1**. Their functional groups, amine and epoxy, could react at 100 °C and form covalent bonds due to epoxy curing reaction [3]. Both APTES and GOPTS were dispersed in pure water by ultrasonic bath with concentrations of 5 v/v % and 1 v/v %, respectively.

2.2.2. Experimental processes
2.2.2.1. VUV activation

Details of VUV activation process are as follows:

(1) Organic cleaned POM substrates were introduced into the VUV/O_3 equipment, of which information is summarized in **Table 2.2**, and the chamber was evacuated to 20 mbar.

(2) The chamber was purged using oxygen to keep purity of the operating gas.

(3) The operating oxygen pressure was controlled at 70 mbar, in consideration of balance between the

Table 2.2 Detail information of VUV/O_3 equipment

Lamp	Xe_2 lamp (Ushio)
Wavelength	172 nm
Distance from lamp	13 mm
Power	10 mW/cm^2

VUV powers reaching POM substrate and consumed by dissociating oxygen, according to Lambert-Beer Law [4].

(4) The VUV/O_3 irradiation was carried out with process times of 30, 60, 150, and 300 s, respectively. During the irradiation, C-O main chains were dissociated and dangling bonds were created on the POM surface.

(5) The chamber was opened for atmosphere.　By this operation, water molecules in atmosphere could react with activated dangling bonds on the POM surface and form a hydrate bridge layer with hydroxyl groups.

2.2.2.2. SAM modifications

POM substrates activated by VUV/O_3 were immersed into either prepared APTES or GOPTS solutions for 20 min, respectively, in order that the methyl groups of SAMs could react adequately with hydroxyl groups on the POM surface.　After the SAM modifications, the POM substrates were rinsed by ethanol and pure water, subsequently, to eliminate the residual excess SAMs and possible organic contaminations on the surfaces and dried by a N_2 gun.

2.2.2.3. Bonding process

The APTES and GOPTS modified substrates were face-to-face contacted and introduced into a bonding equipment (SB6e, SUSS).　Then, the bonding was carried out at 100 °C with an applied

pressure of 3 MPa in N_2 atmosphere for 15 min.

2.2.3. Evaluation methods

2.2.3.1. Surface morphology

Changes in the POM surface morphology were observed by atomic force microscope (AFM, Shimadzu SPM-8000FM) and scanning electron microscope (SEM, Hitachi SU8200). AFM scanned on a 10 × 10 or a 30 × 30 μm^2 area with frequency of 1 Hz. Parameters Ra and Rz were measured by AFM to evaluate surface roughness. Ra is the arithmetical average value of absolute distances of peaks and valleys from the center line within the sampling length, and Rz is the average of maximum peak to valley vertical distance within 5 sampling length. SEM observation was carried out at acceleration voltage of 5 kV.

2.2.3.2. XPS analysis

X-ray photoelectron spectroscopy (XPS, ULVAC-PHI ESCA 1800MC) analysis was carried out to clarify conditions for POM surface binding. Detail information of XPS analysis was summarized in **Table 2.3**. At first, the analyzed POM substrates were organically cleaned and then prepared with the following conditions:

(1) 0/ 60/ 300 s VUV/O_3 irradiation.

(2) APTES modification (after 60 s VUV/O_3 irradiation).

Table 2.3 Detail information of XPS analysis

X-ray source	Mg Kα
Power	400 W
Take-off angle (analysis depth)	45° (2.4 nm, λ taking 3.4 nm)
Pass energy	23.5 eV

(3) GOPTS modification (after 60 s VUV/O$_3$ irradiation).

During the XPS analysis, the chamber was evaluated at 10^{-6} Pa level to reduce influence from outgassing due to POM degradation.   The spectrum analysis was carried out using MultiPak software (ULVAC-PHI).   O 1s (532.8 eV) was used as a reference shift spectrum.   Background subtraction was liner type and each spectrum were fitted using a synthetic Gaussian (90%)-Lorentzian (10%) components.

2.2.3.3. Bonding evaluation method

Bonding strength was evaluated using a manual shear connecting with a digital force gauge (LTDDPX-50T, IMADA Co.).   The maximum shearing force just before fracture was recorded.   After the fracture, SEM observation on a fractured surface was also carried out.

2.3   Results and discussions

2.3.1. Surface analyses results
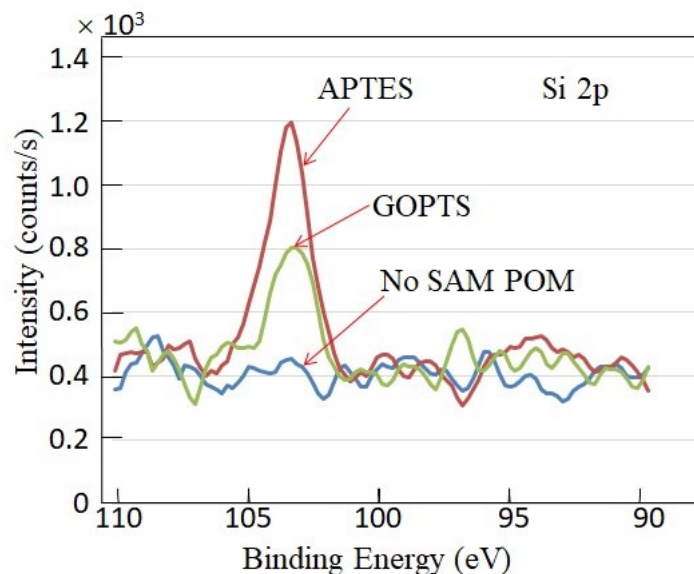
Fig. 2.1 Si 2p spectra of 60 s VUV/O$_3$ treated POM and APTES/GOPTS modified POM (after 60 s VUV/O$_3$ treatment) [2] Copyright (2018) The Japan Society of Applied Physics

2.3.1.1. XPS analysis results

Fig. 2.1 shows overlay curves of Si 2p spectra for a 60 s VUV/O₃ treated POM surface, and APTES/GOPTS modified POM surfaces (after 60 s VUV/O₃ treatment) [5]. No obvious Si peak was observed on the VUV/O₃ treated POM surface while Si peaks occurred on both APTES and GOPTS modified POM surfaces. Since Si element was contained in SAMs, it was confirmed that APTES and GOPTS modifications were successful on POM surfaces.

Fig. 2.2 shows the valence band spectra on VUV/O₃ treated POM surface. A shift of approximate 2.0 eV on O 2p orbit spectra was observed [6-9]. The O 2p orbit shift represented that the POM surface became more electro-conductive, which indicated a carbon condensation due to VUV dissociating POM surface. Double peaks at 4.9 and 2.9 eV could be observed on untreated POM, of which the peak at 2.9 eV was considered to come from organic contaminations because it disappeared after the VUV/O₃ treatment.
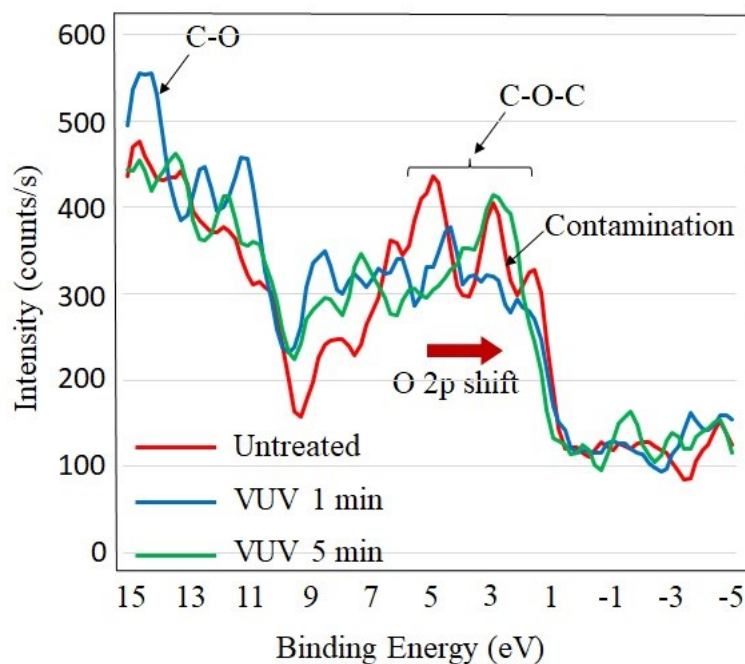
Fig. 2.2 Valence band spectra of POM after 0/60/300 s VUV/O₃ treatment

19

2.3.1.2. Surface morphology analysis results

Fig. 2.3 shows SEM images of POM surfaces treated by VUV/O$_3$ with process times of 0, 30, 60, 150, and 300 s, respectively.   From **Fig. 2.3(a)~(e)**, it could be observed that pore quantity increased with the VUV/O$_3$ process time, which was due to VUV dissociating POM chemical bindings.   A parameter, surface pore area ratio (SPAR), was introduced to evaluate the surface morphology of POM substrate.
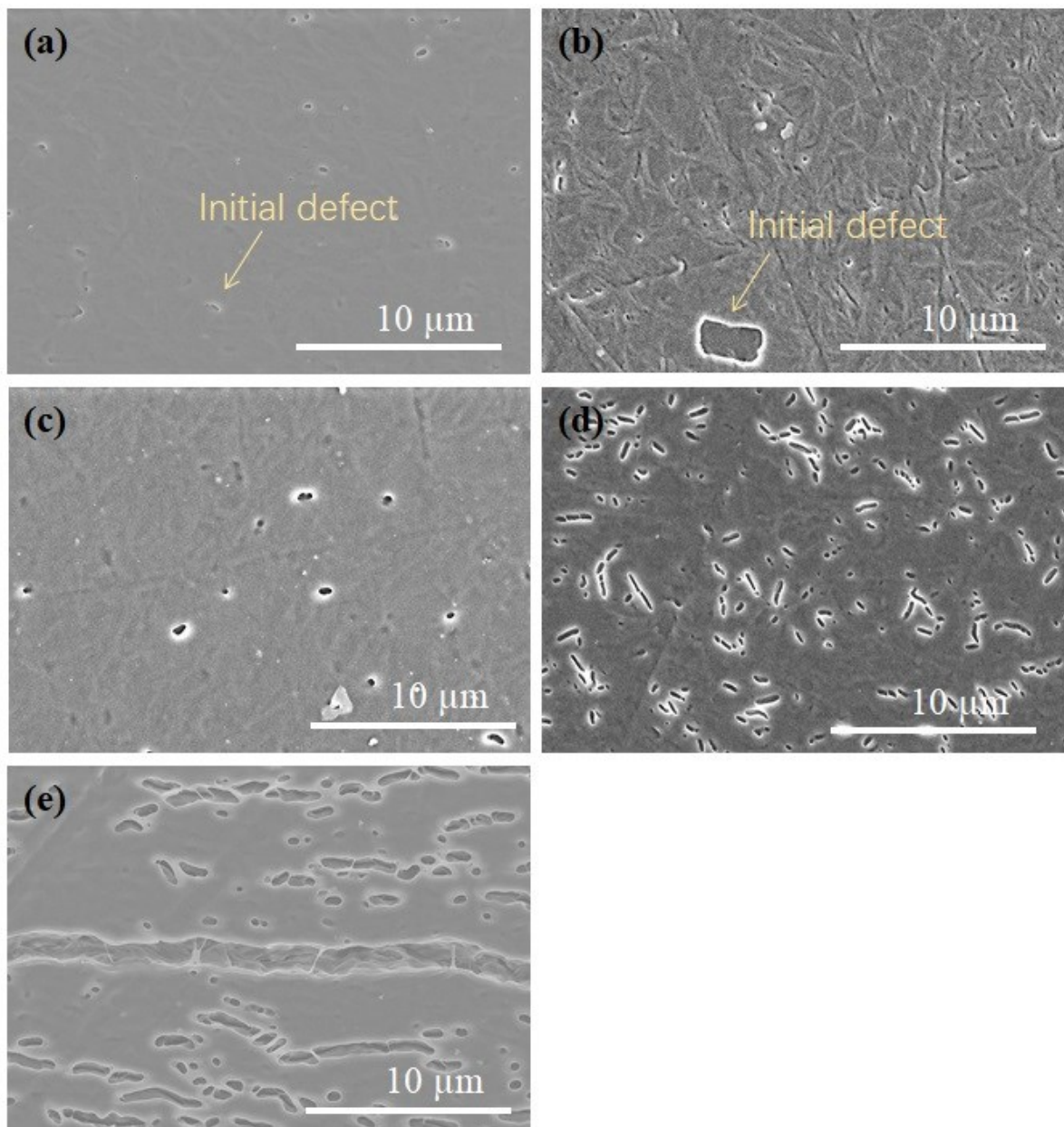
Fig. 2.3 SEM images of the POM surfaces after (a) 0 s; (b) 30 s; (c) 60 s; (d) 150 s; and (e) 300 s of the VUV/O$_3$ treatment [2] Copyright (2018) The Japan Society of Applied Physics

The SPAR was defined as ratio of surface pore area to the total surface area, which was calculated from the SEM images by photoshop software (Adobe).   The calculation showed SPARs were 0.14, 0.93, 0.83, 6.6, and 17 % for the treatment time of 0, 30, 60, 150, and 300 s, respectively.   The 30 s irradiated substrate had an SPAR at the same level with the 60 s irradiated one.   When the irradiation extended over 60 s, the surface pore area expanded strikingly.   This phenomenon was considered that the VUV photonic energy was consumed by removing organic contamination within the first 60 s irradiation, which also well agreed with XPS valence band analysis that organic contamination peak disappeared after the 60 s VUV/O$_3$ treatment.

AFM scanning showed that although the surface roughness Ra and Rz increased from 13.3 and 134.2 nm to 26.9 and 312.2 nm, respectively.   On the other hand, the area without any pores had Ra and Rz of 21.2 and 139.5 nm.   The AFM results confirmed that the dissociation on POM surface was anisotropic, which was due to semi-crystalline of POM.

2.3.2. Bonding results

2.3.2.1. Bonding strength

The bonding strength was calculated using the shear force divided by nominal bonded area A$_{nominal}$. The nominal bonded area could be calculated using the following equation:

$$A_{nominal} = (1 - \alpha)^2 \times A_{total} \tag{2.1}$$

where A$_{total}$ was total bonded area which equaled to the POM surface area, and α was the SPAR calculated

Table 2.4 Shear strengths in term of VUV/O$_3$ process time

VUV/O$_3$ process time	Average strength	Standard deviation
0 s	Not bonded	-
30 s	193 kPa	38.2 kPa
60 s	372 kPa	123 kPa
150 s	81.9 kPa	33.0 kPa
300 s	Not bonded	-

in 2.3.1.2 section.   There was a square of $(1-\alpha)$ as a coefficient in the equation because both APTES and GOPTS modified substrates were treated by VUV/O_3, and thus both bonded substrate surfaces had pores.

The shear strengths were summarized in **Table 2.4** by average bonding strength and standard deviation. It could be observed that the strength increased with the VUV/O_3 treatment until the highest average strength of approximately 372 kPa was obtained at the 60 s irradiation time.   When the irradiation time further extended, the strength decreased, and the 300 s VUV/O_3 treated POM failed to bond.   These results well agreed with the valence band analysis and the SEM surface morphology observation that VUV dissociation effect on the POM surface was prevented by contamination removal, and became striking due to a degradation when the irradiation time extended over 60 s.   In addition, the non-VUV/O_3 treated samples failed to be bonded.   This was considered that the surface modification was not sufficient because of poor chemical groups on POM which could react with SAMs.

2.3.2.2. Theoretical strain energy release rate

In order to further evaluate the bonding, interfacial strain energy release rate was calculated using a theoretical model.   The model assumed that:

(1) The nominal bonded area was concentrated at center of the bonding substrate with area S.

(2) Crack only extended from edge of the bonded area to the center.

(3) All the consumed energy was applied in crack extent, and other energy consumption activities such as plasticity were ignored.

From definition, the strain energy release rate satisfied the following equation [10]:

$$G = -\frac{\partial(U - V)}{\partial A} \tag{2.2}$$

where G was the strain energy release rate, and A was the crack area.   Total bonding energy U and work associated with external forces V could be calculated by:

$$U = \frac{\sigma^2}{2E} SL \tag{2.3}$$

$$V = \frac{\sigma^2}{2E} AL \tag{2.4}$$

in which, σ was the applied stress in shear test, E was Young's modulus, and L was the thickness of the substrates. Obviously, the total bonding energy U was a constant, thus for homogeneous material the strain energy release rate could be written as:

$$G = \frac{\sigma^2}{2E} L \tag{2.5}$$

Therefore, the nominal and real interface strain energy release rate was:

$$G_{nominal} = \frac{\sigma^2}{2E} L \tag{2.6}$$

$$G_{nominal} = \Omega G_{real} \tag{2.7}$$

where Ω was the ratio of a real bonded area to a nominal bonded area. The value of Ω was between 0 and 1, and here it was estimated to be 0.1 for the sake of calculation simplification.

The highest bonding strength of 372 kPa corresponding to the interfacial strain energy release rate of 51.3 mN/m, which was at same level with the surface free energy of POM (38 mN/m). Although the value of strain energy release rate was higher than the POM surface free energy, it was considered as a result of ignoring the energy consuming activities such as plasticity. It could be concluded that the bonding interface reached limit of the theoretical energy in POM.

2.3.2.3. Fractured surface observation

SEM observations of the fractured surfaces are shown in **Fig. 2.4**. **Fig. 2.4(a)** shows the fractured surface of the 60 s irradiated POM surface. It could be observed that a membrane layer was remained on the fractured POM substrate. This membrane was considered to be low molecular weight oxide material (LMWOM) as a result of surface carbon condensation [11-17]. **Fig. 2.4(b)** shows the fractured
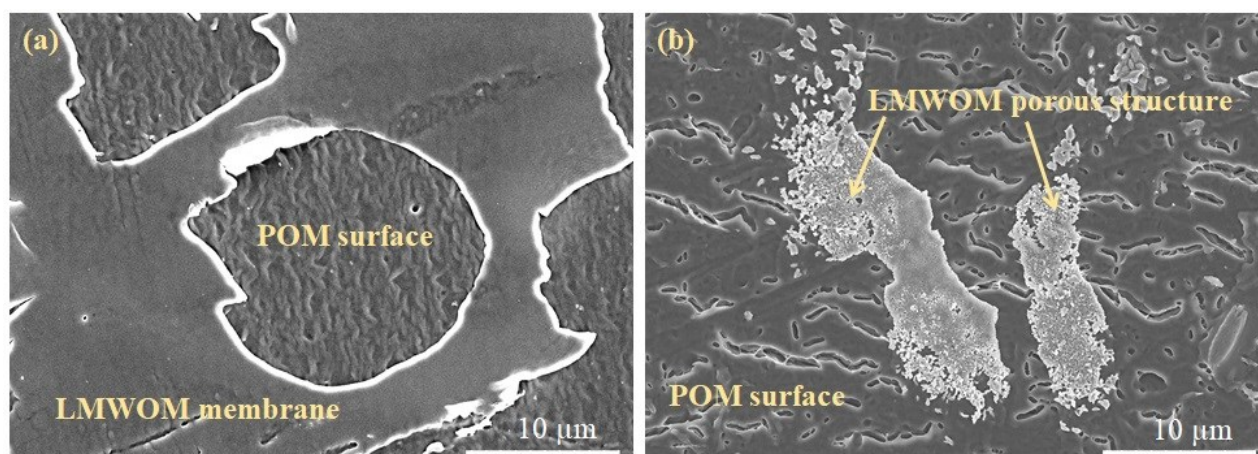
Fig. 2.4 SEM images of the fractured POM surfaces at (a) the 60 s VUV/O$_3$ process time (membrane); and (b) the 300 s VUV/O$_3$ process time (porous structure) [2] Copyright (2018) The Japan Society of Applied Physics

surface of 300 s irradiated POM surface, where the LMWOM remained on the substrates had an appearance of a porous material. This phenomenon further indicated that the excessive VUV/O$_3$ treatment caused degradation of the POM surface as mentioned in 2.3.2.1 section. Since the bonding mechanism on both interfaces was amine-epoxy curing reaction, the interfaces achieved by the different irradiation time conditions should have same strength, which was opposite to our shear strength results. Thus, the bonding strength was affected by the strength of the LMWOM layer. From the bonding strength, it could be concluded that the porous material had lower strength than the membrane. Therefore, it was considered that the porous material had a lower compactness than the membrane.

2.4   Conclusions

This chapter was about the development of a bonding method using VUV irradiation and SAM bridge formation for POM. In this chapter, a POM direct bonding was successfully achieved at 100 °C. APTES and GOPTS were applied as the amine and epoxy bridges on a pair of bonding surfaces, respectively. The XPS analyses results showed that there were Si 2p spectra on the modified surfaces, which were included only in APTES and GOPTS layers. Moreover, SEM and XPS observation results

presented the pore formation during the VUV surface modification according the irradiation time. The pore formation started to occur just after the initial surface contamination was eliminated, hence an excessive VUV irradiation resulted in the dissociation of POM C-O chain that derived a reduction of bond strength. Therefore, we found that there was an optimum irradiation time at around 60 s for POM, where only the initial contamination was removed. Based on a strain release energy model of a crack propagation, the highest bonding strength at optimized irradiation time reached 372 kPa, which corresponded to a strain release energy rate of 51.3 mN/m. Although the values of this calculation tended to be higher than actual due to the assumptions for calculation, we could mention that the bond strength was as high as the POM theoretical limit energy of 38 mN/m (i.e. the bulk fracture energy).

This technology demonstrated the world first low temperature POM bonding. It opened new possibilities for POM future applications in bio-MEMS packaging. It also provided possibilities for direct bonding of polymers with low operating temperatures. By modifying metals using the same method, a hybrid bonding between POM-metal could also be expected in near future.

Reference

[1] L. Tang, N. Y. Lee, Lab Chip, 10 (2010) 1274.

[2] W. Fu, B. Ma, H. Kuwae, S. Shoji, J. Mizuno, Jpn. J. Appl. Phys., 57 (2018) 02BB01.

[3] M. Pramanik, E. W. Fowler, J. W. Rawlins, J. Coatings Technol. Res., 11 (2014) 143.

[4] Y. Naganuma, S. Tanaka, C. Kato, T. Shindo, J. Ceram. Soc. Jpn., 112 (2004) 599, [in Japanese].

[5] J. F. Moulder, W. F. Stickle, P. E. Sobol, K. D. Bomben, "Handbook of X-ray Photoelectron Spectroscopy" (Physical Electronics, Eden Prairie, MN,1992) p. 14.

[6] P. Boulanger, R. Lazzaroni, J. Verbist, J. Delhalle, Chem. Phys. Lett., 129 (1986) 275.

[7] S. R. Cain, Chem. Phys. Lett., 143 (1988) 361.

[8] M. Deleuze, J. Delhalle, D. H. Mosley, J. M. Andre, Physica Scripta, 51 (1995) 111.

[9] P. Boulanger, J. Riga, J. Delhalle, J. J. Verbist, Polymer, 29 (1988) 797.

[10] A. A. Griffith, Philos. T. Roy. Soc. A, 221 (1920) 163.

[11] H. Shinohara, T. Kasahara, S. Shoji, J. Mizuno, J. Micromech. Microeng., 21 (2011) 085028.

[12] H. Shinohara, J. Mizuno, S. Shoji, Sens. Actuators A, 165 (2011) 124.

[13] M. R. Davidson, S. A. Mitchell, R. H. Bradley, Surf. Sci., 581 (2005) 169.

[14] F. A. Rasoul, D. J. T. Hill, J. S. Forsythe, J. H. O'Donnell, G. A. George, P. J. Pomery, P. R. Young, J. W. Connell, J. Appl. Polym. Sci., 58 (1995) 1857.

[15] F. Truica-Marasescu, M. R. Wertheimer, Macromol. Chem. Phys., 206 (2005) 744.

[16] Y. Kim, Y. Taniguchi, K. Murase, Y. Taguchi, H. Sugimura, Appl. Surf. Sci., 255 (2009) 3648.

[17] R. M. Mahfouz, M. Sauer, S. T. Atwa, R. I. Kaiser, K. Roessler, Nucl. Instrum. Methods Phys. Res., Sect. B, 65 (1992) 447.

Chapter 3

POM-PMMA room temperature bonding

This chapter elaborates a room temperature direct bonding between POM and PMMA. In specific POM application, such as dental implant, a room temperature was expected to avoid scald. To achieve such bonding, PMMA was introduced because the ketone groups in PMMA could react with amine at room temperature and PMMA itself was a bio-inert polymer material. The POM surface was modified using amine-terminated SAM. The PMMA was prepared as a semifluid mixture, and thus it could glue into pores on POM, which were formed by VUV dissociation. The bonding was formed by simple drying of the semifluid PMMA. Comparing with the POM bondings, the bonding strength was reinforced by the proposed method because of the anchoring effect. A theoretical calculation estimated that the interface between POM and PMMA had a strain release energy of 32 mN/m, which was at the same level with both POM and PMMA theoretical limit energies. The proposed method was expected to be applied in practical dental therapy.

3.1 **Introduction**

In Chapter 3, a direct bonding method at room temperature between poly-oxymethylene (POM) and poly-methyl methacrylate (PMMA) was proposed.

As mentioned in chapter 2, POM required a low temperature bonding because of its poor heat resistance (i.e. low operating temperature) [1].   Especially, in fields such as dental applications [2-4], in order to avoid scald, the practical temperature had to be precisely controlled within a margin of safety, such as room temperature.   To further decrease the bonding temperature, the designed functional groups had to be reactive also at room temperature.   PMMA was a polymer which was conventionally used in dental therapy.   Thus, PMMA was introduced into the bonding because it contained ketone functional groups that could react with amine groups on the self-assembled monolayer (SAM) modified POM surface by nucleophilic addition reaction at room temperature.

In this chapter, preparation of PMMA would be described, and the bonding would be discussed in terms of the bonding strength and the interfacial strain release energy.

3.2 **POM-PMMA bonding method**

3.2.1. Materials preparation methods

The POM substrate was prepared as described in chapter 2.   The SAM that provided amine groups in this experiment was (3-aminopropyl)triethoxysilane (APTES).   The preparation of APTES solution was also described in chapter 2.

PMMA was prepared using a dental adhesive resin cement (super-bond C&B, sun medical), which contained: polymer powder, monomer and catalyst.   The major constituent of the polymer powder was PMMA.   The major constituents of monomer were methyl methacrylate (MMA) and 4-methacryloyloxyethy trimellitate anhydride (4-META), which could be polymerized to PMMA under
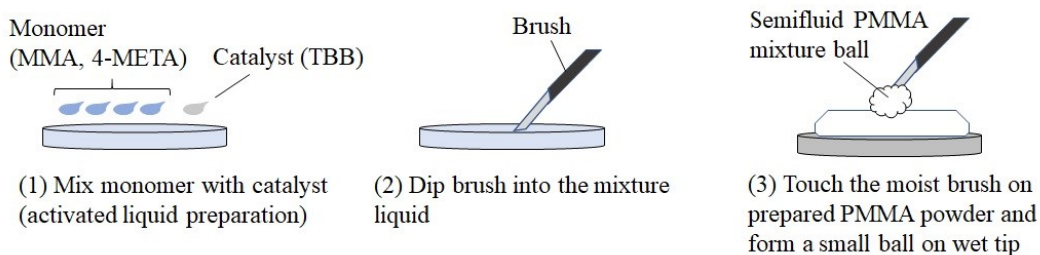
Fig. 3.1 PMMA preparation process

acceleration of partly oxidized tri-n-butyl boron (TBB, i.e. the catalyst).   The preparation process is

shown in **Fig. 3.1** as follows:

(1) Preparing the PMMA powder in a dispensing dish.

(2) Mixing 4 drops of the monomer with 1 drop of the catalyst in another dispensing dish.

(3) Dipping a brush into the mixture of the monomer and the catalyst.

(4) Touching the moist brush to the PMMA powder and form a small ball on the wet tip.

The small ball on brush was semifluid mixture of PMMA, MMA, 4-META and TBB, which further

polymerized to a PMMA bulk.   It included a little impurity when it totally dried out.   In the step (2),

the mixed liquid would be wasted within 5 min from it was created for the sake of quality guarantee.

3.2.2. Surface modification and bonding process

The VUV treatment was carried out in presence of oxygen (i.e. VUV/O$_3$) as described in chapter 2.

The process times were controlled at 30, 60, 300 and 600 s.   The APTES modification process was the

same as described in chapter 2.

Bonding process was simply embedding the semifluid mixture onto the SAM modified POM.

Reaction between ketone groups in PMMA and amine groups on POM surface was a nucleophilic

addition reaction, and the product was imine.   In order to evaluate the bonding strength, the semifluid

mixture was filled into a mold, and form a PMMA bump on the POM substrate as shown in **Fig. 3.2** as

follows:

29

(1) Fix the SAM modified POM with the mold

(2) Embed the hole with semifluid PMMA mixture

(3) Dry and push the PMMA bump out of mold
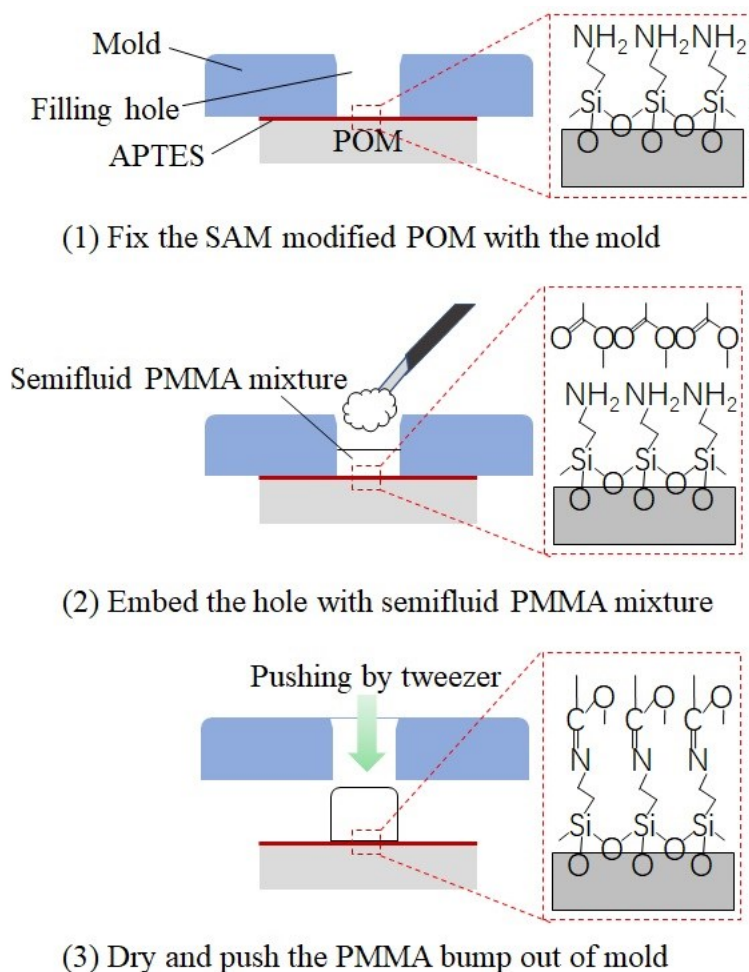
Fig. 3.2 PMMA bump formation process on the SAM modified POM surface

(1) Filling the mold with the semifluid mixture until the 2-mm-diameter hole was embedded.

(2) Drying the semifluid mixture for 30 min to form a PMMA bump.

(3) Pushing the PMMA bump out of mold using a tweezer.

3.2.3. Evaluation methods

X-ray photoelectron spectroscopy (XPS) analysis confirmed the SAM modification on the POM surface. Since the XPS analysis was discussed in chapter 2, the results would not be mentioned in this chapter. The bonding strength was evaluated using the manual shear apparatus, and the POM surface morphology after the fracture was analyzed by scanning electron microscope (SEM), of which the processes were as mentioned in chapter 2.

Table 3.1 Shear strength of POM-PMMA in term of the VUV/O_3 process time

VUV/O_3 process time	Average strength	Standard deviation
30 s	1.04 MPa	0.90 MPa
60 s	2.64 MPa	1.20 MPa
300 s	8.54 MPa	3.72 MPa
600 s	4.75 MPa	0.14 MPa

3.3   Results and discussions

The shear strengths were summarized in **Table 3.1** by average strength and standard deviation.   The strength increased with the VUV/O_3 process time until the highest strength of 8.54 MPa was obtained at 300 s.   With the process time further increasing, the strength decreased.   Comparing with the POM direct bonding as mentioned in chapter 2, the strengths increased as well as the optimized condition shifted to a longer process time (i.e. a larger irradiation dose).   The reason for this tendency was considered to be interface reinforcement due to the semifluid mixture of PMMA embedding into the pores on POM surface.   This phenomenon was called "anchor effect", which was widely applied in adhesive bondings [5, 6].

A simple calculation model was established to evaluate the bonding strain release energy as shown in **Fig. 3.3**.   The strain release energy could be considered as energy required to create two new surfaces from the bonding areas.   In the model, it was assumed that:

(1) The pores on POM were cylinders with a height h and an cross-area a.

(2) The dissociation only enlarged the cylinder bottom area a but not deepen the height.

(3) All the cylinders would be completely embedded with PMMA, and there were no voids or cracks throughout the interface.

(4) Created new surfaces were flat ones.

(5) Possible degradation beneath the pores was ignored.
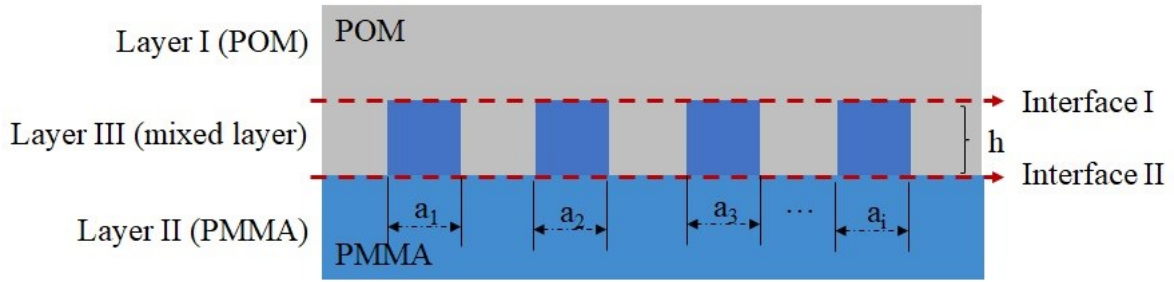
Fig. 3.3 A strain release energy calculation model

In **Fig. 3.3**, the bonding area has 3 different layers (i.e. a POM layer, a PMMA layer, and a mixed layer, marked as layer I, II, and III, respectively) and 2 different interfaces, marked as interface I and II, respectively.   The energies required to create new surfaces could be calculated as follows:

$$E_{Layer\ I} = \int G_{POM} dS_0 \tag{3.8}$$

$$E_{Layer\ II} = \int G_{PMMA} dS_0 \tag{3.9}$$

$$E_{Layer\ III} = \int G_{POM} dS_{residual} + \int G_{PMMA} dS_{cylinder} \tag{3.10}$$

$$E_{Interface\ I} = \int G_{POM} dS_{residual} + \int G_{interface} dS_{cylinder} \tag{3.11}$$

$$E_{Interface\ II} = \int G_{interface} dS_{residual} + \int G_{PMMA} dS_{cylinder} \tag{3.12}$$

in which, E was the strain release energy of layer I, II and III, as well as interface I and II; G was the strain release energy rate of the POM, PMMA and POM-PMMA interface, which could also use value of surface free energy; S_0 was the total area of the POM surface; $S_{cylinder}$ was the total area of pore on POM surface ($S_{cylinder} = \Sigma a_1 + a_2 + a_2 + a_3 + \ldots + a_i$); $S_{residual}$ was the residual surface area on POM except for the pore area ($S_{residual} = S_0 - S_{cylinder}$).   The strain release energy of the POM-PMMA interface was simply calculated based on the bond energy of the interfacial chemical chain.   During the SAM modification, the POM C-O bindings were dissociated and reacted with methyl groups in APTES, which further reacted with ketone groups in PMMA.   Since the dissociation energy of a chemical chain was determined by the weakest binding in the chain, it could be considered that the dissociation energy of the nucleophilic addition reaction product equaled to the dissociation energy of C-N binding.   For ease of

calculation, the POM-PMMA interface strain release energy rate could be estimated using:

$$\frac{G_{interface}}{G_{POM}} = \frac{e_{C-N}}{e_{C-O}}$$

(3.13)

where e_{C-N} and e_{C-O} represented dissociation energies of C-N and C-O bindings, respectively. The strain release energy rates of the POM, PMMA and POM-PMMA interface were 38, 36, and 32 mN/m, respectively. Substitute the strain release energy rates into the equations 3.1 ~ 3.5, it could be observed that the strain release energies of the layers were higher than that of the interfaces, and thus the cracks only occurred in either interface I or II. From the assumptions, with the increase of cylinder bottom area, strain release energy of the interface I would decrease and that of interface II would increase. Hence, a theoretical maximum energy could be estimated when the strain release energies of interface I and II were the same. The maximum value of equivalent strain release energy rate was calculated to be 34 mN/m while the total pore area reached 60 %.

However, it had to be known that the cylinder height (i.e. pore depth) increased with the VUV/O$_3$ process time, and the POM beneath the pores began to dissociate. SEM images of the fractured POM surfaces at 60 and 300 s VUV/O$_3$ irradiation time are shown in **Fig. 3.4(a) and (b)**, respectively. In **Fig. 3.4(a)**, no obvious pores could be observed whereas the pores propagated beneath the mixed layer as shown in **Fig. 3.4(b)**. Since these dissociation pores decrease the bonding strength, it could be expected that the practical bonding strength would increase by further optimization.
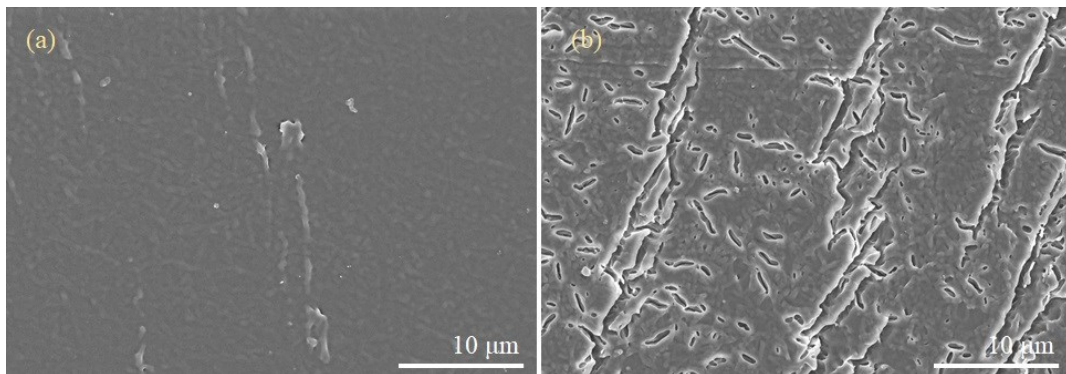
Fig. 3.4 SEM images of the fractured POM substrates at (a) 60 s, and (b) 300 s VUV/O$_3$ process time conditions

34

3.4 **Conclusions**

This chapter mentioned about a room temperature bonding between POM and PMMA, utilizing the results in Chapter 2. The PMMA samples were prepared as a semifluid mixture, and thus it could be filled into pores on APTES modified POM surface. The model calculation indicated the maximum equivalent interfacial strain release energy of 34.4 mJ/m^2, which was comparable with the POM and PMMA theoretical energies of 38 and 36 mJ/m^2, respectively.

The bonding method could provide sufficient strength between bio-inert POM and PMMA materials at room temperature. Therefore, it was expected to be used in practical applications, especially dental therapies.

Reference

[1] W. Fu, B. Ma, H. Kuwae, S. Shoji, J. Mizuno, Jpn. J. Appl. Phys., 57 (2018) 02BB01.

[2] P. Oyar, G. Can, Cumhuriyet Dent. J., 17 (2014) 205.

[3] M. Mishra, S. Ozawa, T. Masuda, F. Yoshioka, Y. Tanaka, J. Adv. Prosthodontics, 3 (2011) 140.

[4] O. Ali, M. Makou, T. Papadopoulos, G. Eliades, Eur. J. Orthodont., 34 (2012) 595.

[5] S. Wang, M. Wang, Y. Lei, L. Zhang, J. Mater. Sci. Lett., 18 (1999) 2009.

[6] M. Yang, Y. Zhao, N. Zhang, Int. J. Rock Mech. Min. Sci., 67 (2014) 96.

Chapter 4

Vapor-assisted VUV surface modification technology

This chapter elaborates a novel vapor-assisted VUV technology for the sake of polymer, such as PEEK, and metal surface modifications. By introducing water vapor into a VUV chamber, hydrogen and hydroxyl radicals could be created through dissociation by VUV. The hydrogen radicals could partly deoxidize metal oxide and create active cation sites on metal surface. These cations would further react with hydroxyl radicals and form hydrate bridge layers. Furthermore, the polymer surface could be dissociated by VUV and then react with hydroxyl radicals to form hydrate bridge layers. XPS detected novel COOH bindings on PEEK surface after the vapor-assisted VUV modification, which confirmed the modification was effective. A theoretical model was established to evaluate the modification effect. It showed that the modification process could be divided into three stages, and the modification effect would be controlled directly by the humidity (i.e. water vapor molecule concentration). An optimized condition was found at 88.0 mmol/m^3 water vapor molecule concentration according to experimental data. The proposed vapor-assisted VUV provided highly compatible modification method for polymer-metal hybrid.

4.1 **Introduction**

In Chapter 4, a surface modification method by novel vapor-assisted vacuum ultraviolet (VUV) was proposed. By applying this method, it was expected that the polymer and metal surfaces could be modified with hydrate bridge layers which could form strong covalent bond through dehydration and condensation reaction at low temperature.

Concept of this method was to modify polymer and metal surfaces utilizing hydrogen and hydroxyl radicals generated by the VUV-dissociated water vapor molecules. Thus, the radical generation rates were considered highly affected by the humidity in an operating chamber. Therefore, in this section, the modification effect was investigated by controlling the vapor molecule concentration, and a theoretical model for the modification optimization was established.

4.2 **PEEK surface modification method**

4.2.1. Vapor-assisted VUV mechanism

Mechanism of the vapor-assisted VUV modification is shown in **Fig. 4.1**. By introducing water vapor into a VUV chamber, hydrogen and hydroxyl radicals were generated through dissociation by VUV. The hydrogen and hydroxyl radicals would react with polymers and metals diversely. In this section, poly-ether ether ketone (PEEK) [1, 2], which was practically applied in hybrid bonding in this thesis, and Cu [3], an oxidable metal conventionally used a wiring metal, were introduced as examples. In Cu surface modification, the mechanism was as follows:

(1) Initial organic contaminations were removed by the VUV irradiation.

(2) Hydrogen radicals would partially deoxidize the surface of Cu oxide, and thus create cation sites.

(3) Hydroxyl radicals reacted on those cation sites, and created a hydrate bridge layer (Cu hydroxyl compound).
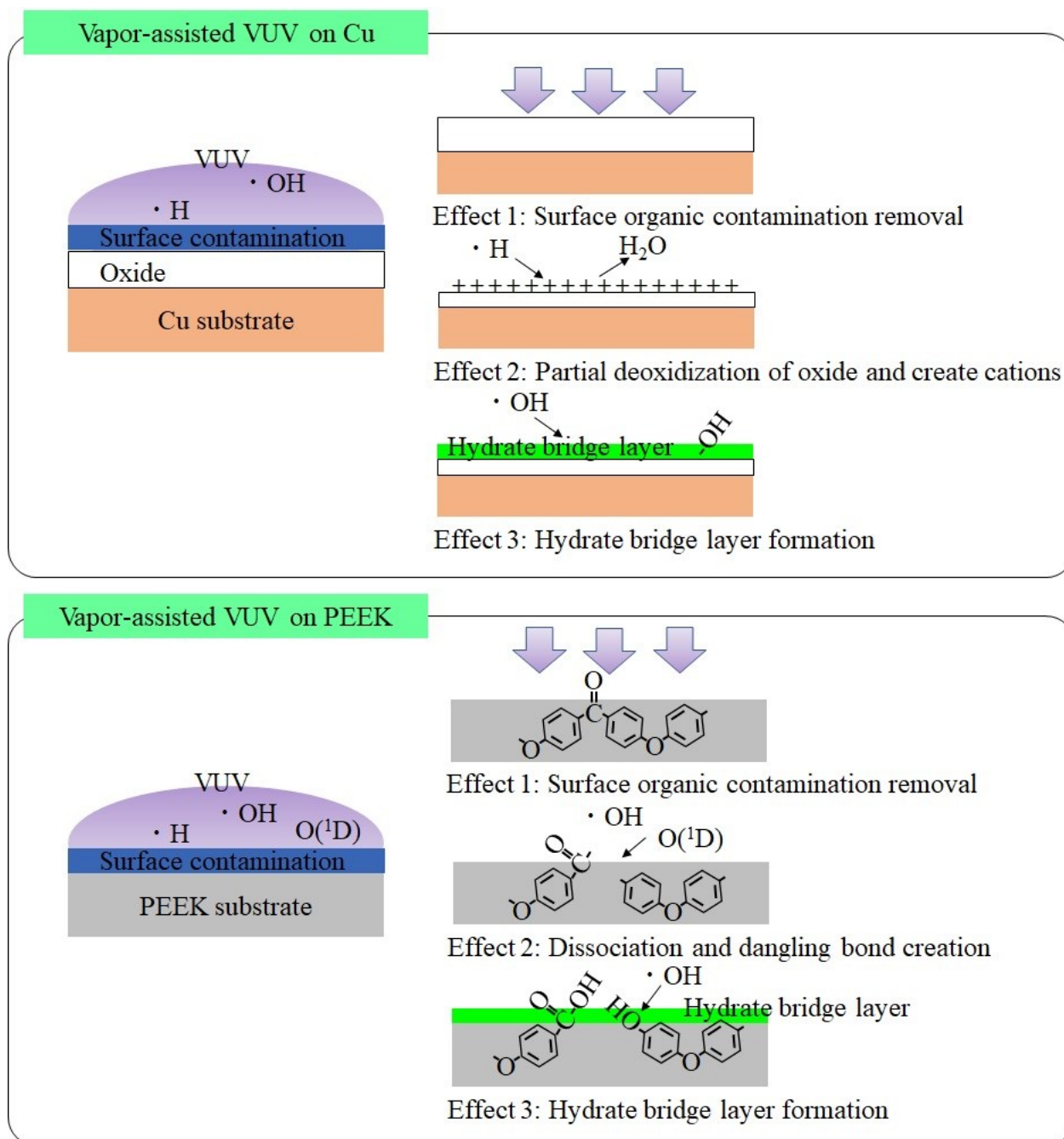
Fig. 4.1 Mechanisms of vapor-assisted VUV on Cu and PEEK

In the PEEK surface modification, the mechanism was as follows:

(1) Initial organic contaminations were removed by VUV irradiation, and hydroxyl radicals were further dissociated into singlet oxygen $O(^1D)$.   The $O(^1D)$ was also created during the metal modifications, however, it did not change the modification products (i.e. hydroxyl compound), and thus it was not discussed.

(2) Chemical bindings were dissociated by the VUV irradiation and the $O(^1D)$ reaction, and therefore reactive dangling bonds were created.

(3) Hydroxyl radicals approached on those dangling bonds, and then created a hydrate bridge layer (hydroxyl and carboxyl groups).

4.2.2. Experimental apparatus

A bonding apparatus is outlined in **Fig. 4.2**.　It consisted of five chambers with discrete vacuum systems: a VUV chamber, a standby chamber, a fast atom beam bombardment (FAB) process chamber, a surface analysis chamber, and a flip-chip bonding chamber.　The VUV chamber was equipped with a 172-nm-wavelength VUV lamp (Ushio), which was positioned 7 cm above the substrate surface.　Detail information of the VUV lamp is summarized in **Table 4.1**.　The standby chamber could store up to 4 samples, and it was maintained at high vacuum level of 10^{-7} Pa.　In the FAB process chamber, a FAB gun (Oxford Applied Research) was located at 7 cm apart from the sample with a 45° incidence angle.
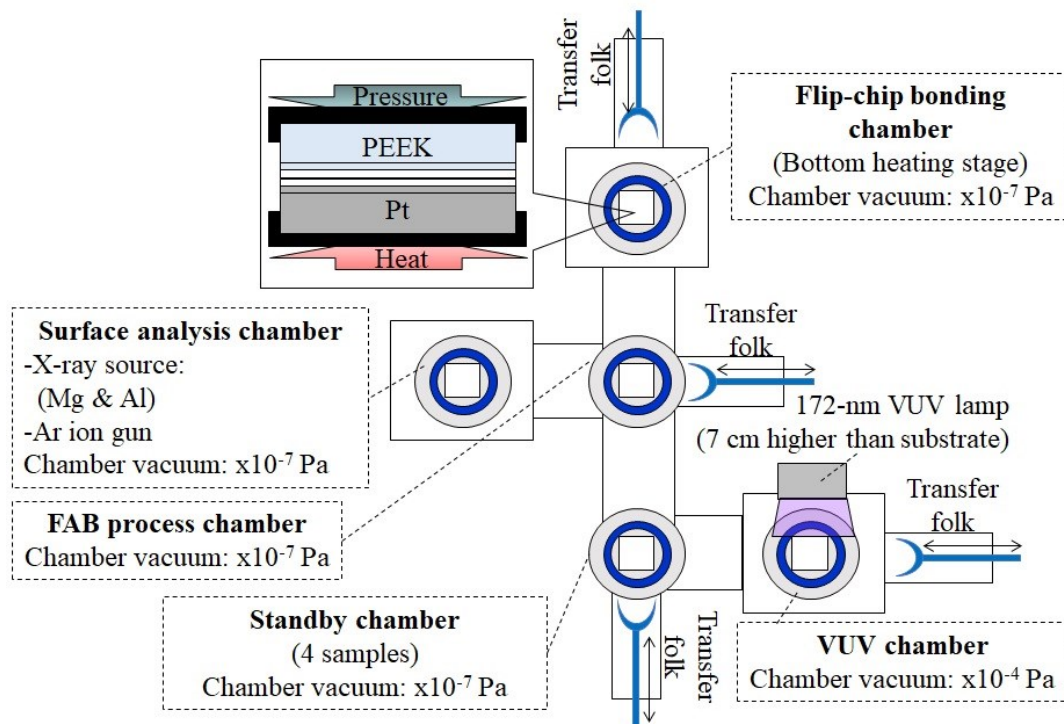
Fig. 4.2 Outline of an experiment apparatus

Table 4.1 Detail information of VUV lamp

Lamp source	Xe_2
Wavelength	172 nm
Distance from sample surface	70 mm
Power	10 mW/cm^2
Operation temperature	Room temperature (about 20 °C)
Pressure (before gas introduction)	1×10^{-4} Pa

The surface analysis chamber was equipped with an x-ray photoelectron spectroscopy (XPS, ESCA 1600, ULVAC-PHI), of which an x-ray source was Al Kα ($hv = 1486.6$ eV).   In the flip-chip bonding chamber, a heater was positioned on bottom of the sample.

4.2.3. Vapor-assisted VUV modification process

Prepared substrates were PEEK which would be further applied also in hybrid bonding.   Dimensions of the PEEK substrates were 10 x 10 mm^2, with thickness of 0.5 mm.   Before the modification, the substrates were organically cleaned in ultrasonic bath in order of ethanol (180 s) and pure water (60 s). Details of the procedure are described as follows:

(1) The organically cleaned samples were introduced into the VUV chamber.

(2) The chamber was evacuated to order of 10^{-4} Pa.

(3) Vacuum pumps of the chamber were stopped.

(4) Water vapor and N$_2$ were introduced into the VUV chamber successively at ratios summarized in **Table 4.2**, until the pressure reached -3 kPa.

(5) The VUV irradiation was carried out for 10 min.

(6) The chamber was evacuated back to 10^{-4} Pa.

(7) The surface modified substrate was transferred into the surface analysis chamber for the XPS analysis.

Table 4.2 Gas concentration conditions according to rations of inlet volume

Condition numbers	Gas inlet (H_2O /N_2, %)	Relative humidity (%)	Irradiation temperature (°C)
PEEK 1	20/80	0.60	20.55
PEEK 2	30/70	3.60	20.55
PEEK 3	40/60	8.80	20.60
PEEK 4	50/50	16.60	20.60
PEEK 5	90/10	64.30	21.00

In this procedure, the VUV irradiation process time was determined by the necessary stable time of our apparatus based on their past performances. During the VUV irradiation, process temperature and relative humidity (**Table 4.2**) were recorded in order to calculate water vapor density and molar concentration. The calculation equations are shown as follows:

$$e_s(\text{T}) = 6.11 \times 10^{\frac{7.5T}{T+237.3}} \qquad (4.14)$$

$$a_s(\text{T}) = \frac{217 \times e(T)}{T + 273.15} \qquad (4.15)$$

$$a(\text{T}) = a_s(T) \times RH \qquad (4.16)$$

$$C_{Total} = a(T) \div M_{water} \qquad (4.17)$$

In the equations, $e_s(t)$ and $a_s(t)$ are saturation water vapor pressure and volumetric humidity (i.e. saturation water vapor density), respectively; $a(T)$ is water vapor density in the chamber; C_{Total} is the total water vapor molecule molar concentration; RH is the relative humidity and T is the temperature during the process. The calculated water vapor densities and water vapor concentrations are also shown in **Table 4.3**.

4.2.4. XPS analyses

Table 4.3 Water density and vapor concentration during the vapor-assisted VUV modification according to rations of gas inlet volume

Conditions	Gas volume (H_2O /N_2)	Water vapor densities	Molar concentrations
PEEK 1	20% / 80%	0.11 g/m^3	0.006 mol/m^3
PEEK 2	30% / 70%	0.64 g/m^3	0.036 mol/m^3
PEEK 3	40% / 60%	1.58 g/m^3	0.088 mol/m^3
PEEK 4	50% / 50%	2.98 g/m^3	0.165 mol/m^3
PEEK 5	90% / 10%	11.80 g/m^3	0.656 mol/m^3

In XPS analyses, the applied power was 450 W, and the pass energy was set at 10 eV.   Spectra were recorded at take-off angles of 15° with respect to surface normal.   Analysis depths corresponding to the take-off angles of 15° was 0.9 nm when inelastic mean free path (λ) was assumed as 3.4 nm in polymer materials [4].   Spectrum analysis was carried out using the MultiPak software (ULVAC-PHI). Backgrounds of the spectra were removed by the Shirley background subtraction mode for peaks of transition metal and the Liner background subtraction mode for ones of non-transition metal.   The spectra curves were fitted using synthetic Gaussian (80%)-Lorentzian (20%) components.

4.3   **Results and discussions**

4.3.1. XPS analyses results

Since bonding was dominated by conditions on a substrate surface, our curve fittings were focused on outmost surfaces (0.9 nm).   **Fig. 4.3(a)~(e)** show C 1s spectra of PEEK outmost surfaces modified by 6.00, 36.0, 88.0, 165 and 656 mmol/m^3 water vapor concentration conditions, respectively.   As a comparison, a C 1s spectrum of an untreated PEEK outmost surface (0.9 nm) is shown in **Fig. 4.3(f)**.   In **Fig. 4.3(f)**, it could be observed that the PEEK surface contained C_xH_y (284.8 eV, from aromatic [5-8]), C-O (286.6 eV, from hydroxyl [5-8]) and C=O (287.7 eV, from carbonyl [5-8]) bindings.   After the vapor-assisted VUV modifications, as shown in **Fig. 4.3(a) and (b)**, novel peaks with energy gap of 0.8 ± 0.1 eV [5-8] occurred which were considered as C-C peak from aliphatic.   These novel aliphatic bindings were considered to come from low molecular weight oxide materials due to carbon condensation

by VUV irradiations [8-16].   In addition, these C-C peaks did not appear when the water vapor concentration was higher than 36.0 mmol/m^3.   The reason for this difference was considered that the VUV photons were totally consumed by water vapor dissociation at this concentration, and thus cannot further dissociate the PEEK chemical bindings.   In **Fig 4.3(a)~(e)**, the C=O peaks transformed into novel peaks with the energy gap of 4.6 ± 0.2 eV from C_xH_y peaks, which were recognized as carboxyl
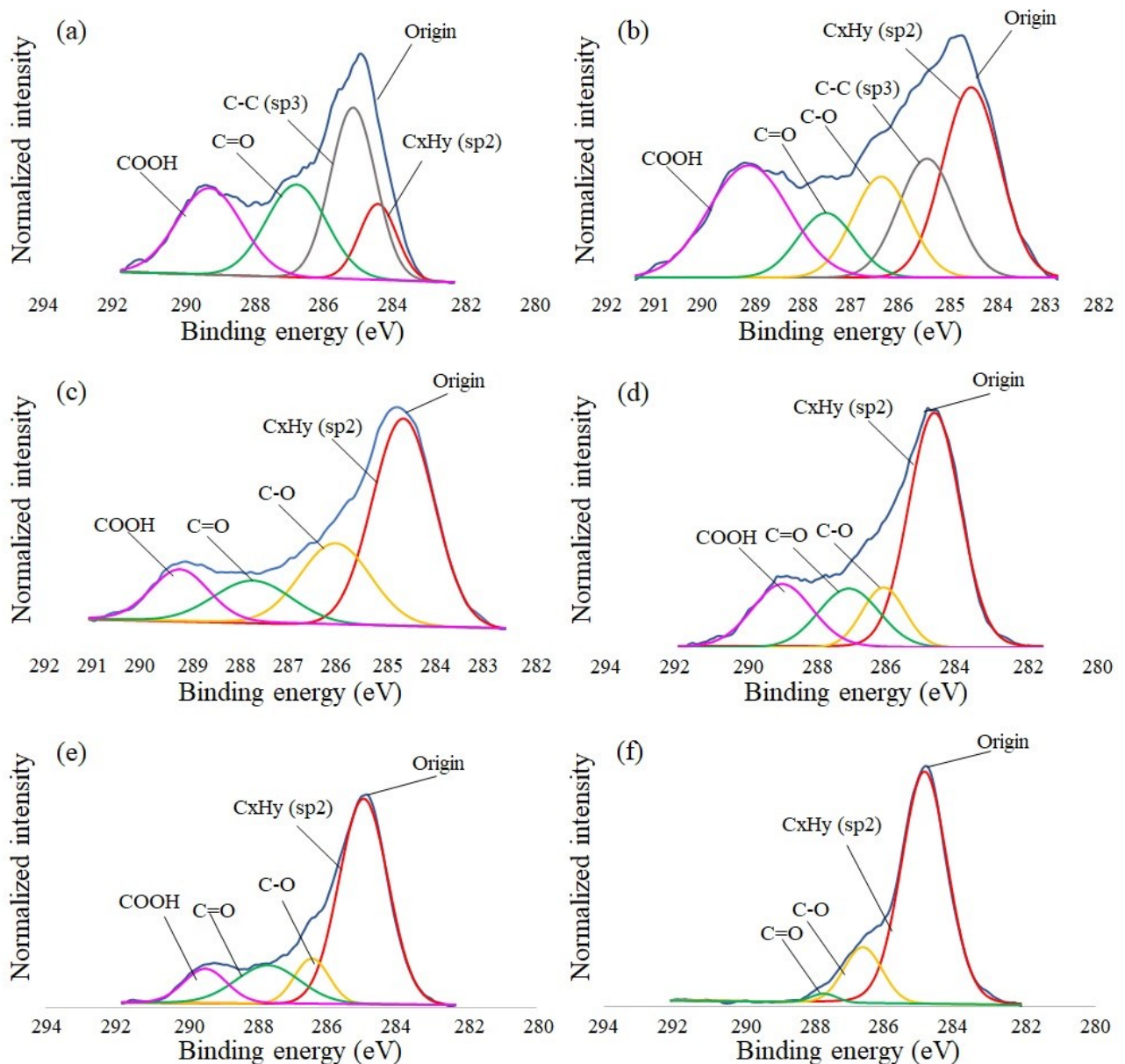
Fig. 4.3 C 1s spectra curve fitting on outmost surfaces (0.9 nm) of: vapor-assisted VUV modified PEEK at (a) 6.00, (b) 36.0, (c) 88.0, (d) 165, (e) 656 mmol/m^3 vapor concentrations, and the reference (f) unmodified PEEK.

groups (i.e. COOH) [5-8].   The formation of COOH was considered to be due to two mechanisms:

(1) Hydroxyl radicals reacted with the VUV-dissociated carbonyl groups.

(2) Hydrogen radicals reacted with carboxylate dangling bonds created from carbonyl groups by singlet oxygen $O(^1D)$.

In addition, hydroxyl functional groups were considered to be formed during the modification.   But its chemical bindings were covered with C-O from the PEEK structure.   Thus, the binding was difficult to be identified.   As a result, the PEEK was successfully modified with carboxyl functional groups on its outmost surface.

4.3.2. Theoretical calculation

4.3.2.1. Atom numeric ratio of O/C

PEEK was consisted of carbon, oxygen and hydrogen.   However, since it was difficult to identify hydrogen directly, the emphasis of this research was laid on carbon and oxygen.   In this section, an equivalent ratio of atomic concentration for O to C (i.e. O/C ratio) was introduced to evaluate surface modification effect.   It could be considered that the modification effect increased with the amount of oxygen contained in PEEK.   Thus, the O/C ratio increased with the modification effect.   Ideal PEEK structure $((-O-C_6H_4-O-C_6H_4-C(=O)-C_6H_4-)_n)$ had 19 carbon atoms and 3 oxygen atoms per monomeric unit.   Thus, the O/C ratio in ideal PEEK was calculated as 0.16.   The O/C ratio in PEEK modified by the vapor-assisted VUV under each vapor inlet condition were summarized in **Fig. 4.4**.   In **Fig. 4.4**, a horizontal axis indicates water vapor concentrations and a vertical axis is the O/C ratios.   It can be observed that the curves have tendency of decreasing with the increase of the water vapor densities except for the area between the two decreases.   Hence, it was considered that the surface modification effect decreased with the increase of the water vapor concentrations.
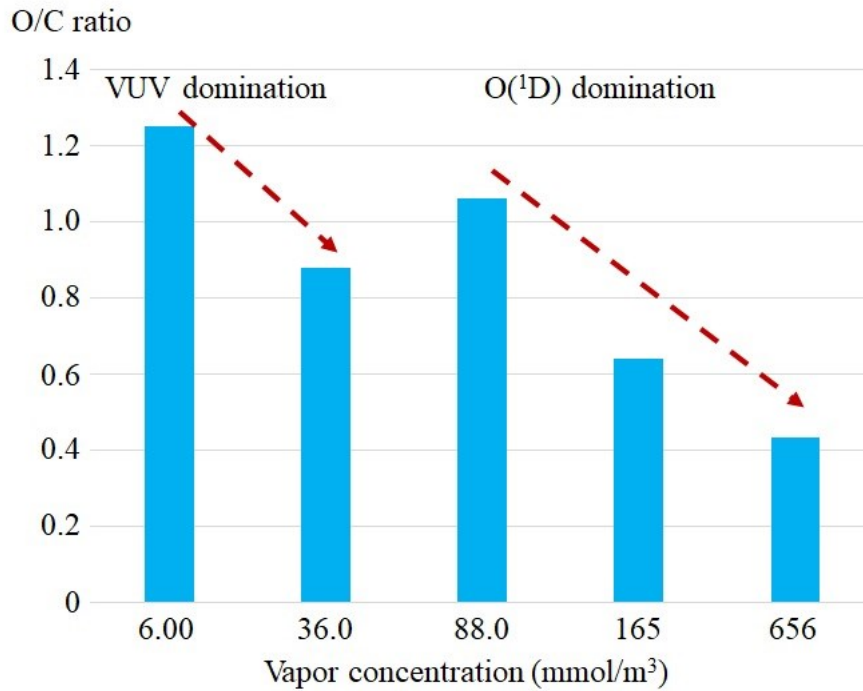
Fig. 4.4 Modification effect evaluated using O/C ratio

4.3.2.2. Calculation of oxygen singlet O(^{1}D) concentration

The O/C ratio tendency could be explained by the Lambert-Beer Law [17], which indicated light attenuation through the material it traveled as the following equation:

$$I = I_0 e^{-\varepsilon cx} \tag{4.18}$$

In the equation, I_0 is irradiance of a VUV lamp and I is the one reached on a substrate surface; ε is a molar attenuation coefficient, c is material molar concentration, and x is irradiation distance. The molar attenuation coefficient was estimated as 2.5×10^7 cm^2/mol from reference data [18. 19]. According to this equation, it could be calculated that the irradiance reached substrate surface was approximate 0.2 % when the water vapor molar concentration was 36.0 mmol/m^3. On the other hand, the irradiance reached on the substrate surface could be assumed to be 0, when the water vapor molar concentration was 88.0 mmol/m^3 and even higher. This result well agreed with the PEEK curve fitting results in section 4.3.1 that the C-C aliphatic peaks did not appear when the vapor concentration reached 88.0

mmol/m^3.　It was considered that the chemical bindings of PEEK would not be dissociated adequately if the VUV irradiance could not reach the substrate surface.　Therefore, an optimization of the inlet water vapor concentration was necessary and since the excessive water vapor may limit the modification effect.

　　To optimize the inlet vapor concentration, a model should be introduced from a specific situation. First, we considered the situation that the VUV energy was totally consumed by the water vapor.　In this situation, we assumed that VUV energy consumed by the water vapor was all costed in water molecule dissociations.　As a simple model, gas molecules and radicals were assumed to disperse uniformly in a chamber.　Moreover, it was assumed that only the following four reactions occurred during the VUV irradiations and the radicals reacted with a substrate were ignored:

$$H_2O + h\nu \rightarrow \cdot OH + \cdot H$$

$$\cdot OH + h\nu \rightarrow O(^1D) + \cdot H$$

$$O(^1D) + \cdot H \rightarrow \cdot OH + heat$$

$$\cdot OH + \cdot H \rightarrow H_2O + heat$$
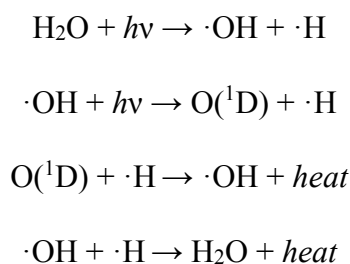
In these reactions, the first two reactions may consume the VUV energy while the last two reactions release heat.　Assuming the energies consumed in both equations were the same for the sake of calculation simplification, it could be defined that a coefficient p represented the possibility at which single H_2O molecule or $\cdot OH$ radical consumed the VUV energy and was dissociated into $\cdot OH$ radical or oxygen singlet $O(^1D)$.　From the definition, it had:

$$p = \frac{\frac{E_{VUV}}{e}}{(c_{OH} + c_{water})V} \tag{4.19}$$

in which, E_{VUV} was the energy consumed by water vapor, e was bond dissociation energy of the O-H bond (taking the value from bond energy of water molecule: 459 kJ/mol), V was chamber volume, c_{OH} and c_{water} were concentrations of $\cdot OH$ radicals and water vapor molecules in chamber, respectively.

Because of the situation that the VUV energy was absolutely consumed by the water vapor, E_{VUV} could be considered as a constant. In this case, in a very short time Δt, the equation 4.6 could be rewrite as:

$$p = \frac{W_{VUV}S\,\Delta t}{e}\frac{1}{(c_{OH}+c_{water})V} = \frac{W_{VUV}}{eh}\frac{1}{c_{OH}+c_{water}}\Delta t = \alpha\frac{1}{c_{OH}+c_{water}}\Delta t \quad (4.20)$$

here, W_{VUV} was the power of VUV source supplied, S was irradiation area, h was distance from a lamp to substrate surface. A mathematic result of W_{VUV}/eh could be converted into a coefficient α because the result was a constant. Integrating p in a very short period of time t_{life}, where t_{life} was defined as lifetime of O(^{1}D), then the concentration of O(^{1}D) could be calculated using the following equation:

$$c_{O1D} = \int_0^{t_{life}} \alpha\frac{c_{OH}}{c_{OH}+c_{water}}dt = \alpha t_{life}\frac{c_{OH}}{c_{OH}+c_{water}} \quad (4.21)$$

When the gas system kept balance, the following equations could be fulfilled:

$$pc_{OH} + \frac{\Delta t}{VN_A}k_{OH}c_{OH} = pc_{water} + \frac{\Delta t}{VN_A}k_{O1D}c_{O1D} \quad (4.22)$$

$$c = c_{water} + c_{OH} + c_{O1D} \quad (4.23)$$

In these equations, k_{OH} and k_{O1D} were reaction rate constants of ·OH to H_2O and O(^{1}D) to ·OH, respectively. Both reaction rate constants had the same units of $L\cdot mol^{-1}s^{-1}$ and they were constants at a given temperature [20-23]. In addition, c was the sum of concentrations of the water vapor, ·OH and O(^{1}D), which was also the initial inlet vapor concentration. According to the reaction equations, c could also be considered as molar concentration estimated in gas inlet conditions (shown in **Table 4.3**) as well as in equation 4.5. Solving equations (8) ~ (10), the result was as follows:

$$c_{O1D} = \frac{2\alpha^3 t_{life}^2 k_{OH}}{VN_A\left[\sqrt{\left(\frac{k_{OH}c}{VN_A}+2\alpha-\frac{\alpha t_{life}k_{O1D}}{VN_A}\right)^2} + \sqrt{\left(\frac{k_{OH}c}{VN_A}+2\alpha-\frac{\alpha t_{life}k_{O1D}}{VN_A}\right)^2 - 4\frac{\alpha^2 t_{life}k_{OH}}{VN_A}}\right]} \quad (4.24)$$

Obviously, the O(^{1}D) concentration c_{O1D} was a function of the water vapor molar concentration c_{total}, and

c_{O1D} decreased with the increase of c.   This calculation results well agreed with the tendency of O/C

ratio, which decreased with the water vapor concentration when the vapor concentration was over 88.0

mmol/m^3, and thus indicated a limited modification effect.

Now, considering a normal situation, the practical consumed VUV power W could be written as

follows:

$$W = (I_0 - I) \cdot S = I_0(1 - e^{-\varepsilon x c}) \cdot S = W_{VUV}(1 - e^{-\varepsilon x c}) \tag{4.25}$$

Substitute W into equation 4.11, it has:

$$c_{O1D} = \frac{2\beta^3 t_{life}{}^2 k_{OH}}{VN_A \left[\sqrt{\left(\frac{k_{OH}c}{VN_A} + 2\beta - \frac{\beta t_{life}k_{O1D}}{VN_A}\right)^2} + \sqrt{\left(\frac{k_{OH}c}{VN_A} + 2\beta - \frac{\beta t_{life}k_{O1D}}{VN_A}\right)^2 - 4\frac{\beta^2 t_{life}k_{OH}}{VN_A}} \right]} \tag{4.26}$$

Where β was α(1-e$^{-\varepsilon x c}$).   By differentiating equation 4.13, there was a maximum value, where c_{O1D} had

a highest concentration.   According to the experiment data, this optimized value was turned out when

the inlet vapor concentration was controlled at 88.0 mmol/m^3.

Considering the O/C ratio with oxygen singlet concentration, it could be concluded that with increase

of humidity (i.e. vapor molecule concentration), there were three stages in the modification:

(1) When the vapor concentration was low, the modification was dominated by the VUV dissociating.

With humidity increasing, VUV energy would be consumed by water molecule dissociation.   Therefore,

the modification effect decreased with vapor concentration.

(2) When vapor concentration further increased, singlet oxygen O(^{1}D) became dominating the

modification.   Since the O(^{1}D) concentration increased with the vapor concentration, the modification

effect also increased with the vapor concentration.

(3) When the vapor concentration was excessive and VUV light energy was totally consumed by water

molecules, with vapor further increasing, the excessive vapor consumed energy that generated O(^{1}D).

Therefore, the modification effect decreased with excessive increased vapor concentration.

4.4 **Conclusions**

This chapter was about the vapor-assisted VUV modification method for PEEK and Pt, whose surfaces were tolerant of dehydration condensation reaction to create the bridge layer.   Firstly, the number of effective radical species on PEEK were theoretically estimated to clarify the mechanism of bridge formation.   In this theory, the bonding process was assumed to include three stages: (1) When vapor concentration was low, the surface modification was dominated by the activation by VUV.   Therefore, corresponding to increasing vapor concentration, the modification effect decreased.   (2) When vapor concentration further increased, singlet oxygen $O(^1D)$ became dominating the modification.   The $O(^1D)$ was created by dissociating hydroxyl radials.   Since $O(^1D)$ concentration increased with vapor concentration, the modification effect increased with inlet number of vapor molecules.   (3) When the humidity became too high and VUV energy was totally consumed by water molecules, the excessive vapor consumed energy that created $O(^1D)$.   Thus, the $O(^1D)$ concentration decreased with vapor concentration, and the modification effect also decreased.   We proved these phenomena happening on the PEEK surfaces from XPS results, and optimized the humidity condition as 88.0 mmol/m^3.

The proposed vapor-assisted VUV modification method provided a strong candidate for future polymer-metal hybrid bondings.   By applying the optimized condition in vapor-assisted VUV modification, the modified polymer surface could form more oxygen-contained groups, such as hydroxyl and carboxyl groups, and thus increase the hybrid bonding strength.

References

[1] W. Fu, A. Shigetou, S. Shoji, J. Mizuno, J.Mater. Sci. Eng. B,, 7 (2017) 49.

[2] W. Fu, A. Shigetou, S. Shoji, J. Mizuno, Mater. Sci. Eng. C, 79 (2017) 860.

[3] A. Shigetou, T. Suga, J. Electron. Mater., 41 (2012) 2274.

[4] C. J. Powell, NIST Electron Inelastic-Mean-Free-Path Database, ver. 1.2, 2010.

[5] J. F. Moulder, W. F. Stickle, P. E. Sobol, K. D. Bomben, "Handbook of X-ray Photoelectron Spectroscopy" (Physical Electronics, Eden Prairie, MN,1992) p. 40

[6] H. W. Tien, Y. L. Huang, S. Y. Yang, J. Y. Wang, C. C. M. Ma, Carbon, 49 (2011) 1550.

[7] G. P. Lopez, D. G. Castner, B. D. Ratner, Surf. Interface Anal., 17 (1991) 267.

[8] H. Shinohara, T. Kasahara, S. Shoji, J. Mizuno, J. Micromech. Microeng., 21 (2011) 085028.

[9] H. Shinohara, J. Mizuno, S. Shoji, Sens. Actuators A, 165 (2011) 124.

[10] M. R. Davidson, S. A. Mitchell, R. H. Bradley, Surf. Sci., 581 (2005) 169.

[11] F. A. Rasoul, D. J. T. Hill, J. S. Forsythe, J. H. O'Donnell, G. A. George, P. J. Pomery, P. R. Young, J. W. Connell, J. Appl. Polym. Sci., 58 (1995) 1857.

[12] F. Truica-Marasescu, M. R. Wertheimer, Macromol. Chem. Phys., 206 (2005) 744.

[13] Y. Kim, Y. Taniguchi, K. Murase, Y. Taguchi, H. Sugimura, Appl. Surf. Sci., 255 (2009) 3648.

[14] R. M. Mahfouz, M. Sauer, S. T. Atwa, R. I. Kaiser, K. Roessler, Nucl. Instrum. Methods Phys. Res., Sect. B, 65 (1992) 447.

[15] Y. Naganuma, S. Tanaka, C. Kato, T. Shindo, J. Ceram. Soc. Jpn., 112 (2004) 599, [in Japanese].

[16] K. Watanabe, M. Zelikoff, J. Opt. Soc. Am., 43 (1953) 753.

[17] K. Watanabe, C.Edward, Y. Inn, M. Zelikoff, J. Chem. Phys. Phys., 21 (1953) 1026.

[18] G. Paraskevopoulos, D. L. Singleton, Rev. Chem. Intermed., 10 (1988) 139.

[19] Wm. Wilson, E. Jr., J. Phys. Chem. Ref. Data, 1 (1972) 535.

[20] K. H. Gericke, F. J. Comes, Chem. Phys. Lett. 81 (1981) 218.

[21] D. Biedenkapp, L. G. Hartshorn, E. J. Bair, Chem. Phys. Lett., 5 (1970) 379.

Chapter 5

PEEK-Pt low temperature direct bonding

This chapter elaborates a low temperature direct hybrid bonding method between PEEK and Pt. The highly compatible vapor-assisted VUV was applied as the surface modification method. The vapor-assisted VUV modified PEEK-Pt bonding was feasible at 150 °C. From the XPS analyses, it could be found that ultrathin hydrophilic bridge layers of Pt hydrate and carboxyl groups on PEEK were successfully created. These layers could generate hydrogen bonds at the moment of contact, and then the bonds were strengthened via dehydration condensation by further heating. The highest bonding strength reached 0.75 MPa corresponding to the strain release energy rate of 2.0×10^{-1} N/m, which was comparable with the theoretical energy of PEEK (i.e. 4.2×10^{-2} N/m). Furthermore, the vapor-assisted VUV modified samples had strengths comparable with ones with conventional methods (FAB modified sample strength: 0.088 MPa; simple VUV modified sample strength: 0.21 MPa) which required high vacuum conditions. The vapor-assisted VUV technology could provide a strong candidate for future polymer-metal hybrid, and was expected to be used in future bio-MEMS applications.

5.1   **Introduction**

In Chapter 5, hybrid bonding between poly-ether ether ketone (PEEK) and Pt through the vapor-assisted VUV was proposed.   Pt had been chosen as an example of bio-inert wiring metal.   Note that the vapor-assisted VUV method is available to other bio-compatible metals such as Ti.

Aim of this chapter, was to realize a low temperature direct hybrid bonding method for packaging of a biomedical micro electromechanical system (bio-MEMS).   As mentioned in Chapter 1, in the bio-MEMS packaging, the hybrid between polymer-metal had the three different interfaces (i.e. a polymeric interface, a metallic interface, a polymer-metal interface) that had to be bonded simultaneously, so that both polymer and metal must be modified at the same time.   The proposed vapor-assisted VUV was not only a low temperature process, but also a highly compatible one that could create hydrate bridge layers on both surfaces of polymer and metal [1].   These hydrate bridge layers could form covalent bonds directly through dehydration and condensation reactions at low temperature.   Furthermore, the vapor-assisted VUV could be carried in atmospheric pressure.   Therefore, the vapor-assisted VUV had a process advantage over conventional ones under high vacuum condition, such as fast atom beam bombardment (FAB) [1, 2].

In this section, the vapor-assisted VUV modification effect on the PEEK-Pt hybrid bonding would be estimated.   By comparison, the conventional FAB and the simple VUV were introduced as reference methods.

5.2   **PEEK and Pt modification methods**

5.2.1. Materials preparation

Dimensions of the PEEK and Pt (purity $\geq$ 99.5 %) substrates were 10 x 10 mm^2, with the thickness of 0.5 and 0.3 mm, respectively.   The substrates were physically polished before the experiments in order

Table 5.1 Surface roughness before and after physical polishing

	Before polishing		After polishing	
	Ra (nm)	Rz (nm)	Ra (nm)	Rz (nm)
Pt	41.6	392.4	4.2	53.2
PEEK	25.9	152.3	1.7	36.8

to create a uniform initial surface morphology.   Surface roughness was measured by an atomic force microscopy (AFM, Shimadzu).   The roughness of the measured area was 500 nm x 500 nm for each substrate with two roughness parameters: Ra and Rz, and the results were summarized in **Table 5.1**. Organic cleaning was carried out in an ultrasonic bath in order of acetone (180 s), ethanol (180 s) and pure water (60 s) for Pt, and ethanol (180 s), pure water (60 s) for PEEK.

5.2.2. Vapor-assisted VUV process

The vapor-assisted VUV process was the same as mentioned in chapter 4.   The vapor concentrations were controlled at 36.0, 165 and 656 $mmol/m^3$ for evaluation of the Pt surface modification.   As in the hybrid bonding, the vapor concentrations were controlled at 36.0 and 656 $mmol/m^3$ for a simple comparison of modification effects between low and high humidity conditions.

5.2.3. FAB and simple VUV process

The FAB procedure was as follows:

(1) The substrate was introduced into a FAB process chamber.

(2) The stage began to rotate in order that the surface was uniformly treated.

(3) The chamber was purged using flux-controlled Ar gas.

(4) Process current and voltage were adjusted to 20 mA and 2 kV, respectively.

(5) The process lasted for 10 min.

The simple VUV procedure was as follows:

(1) The substrate was introduced into a VUV chamber.

(2) The VUV chamber was evacuated to the order of 10^{-4} Pa.

(3) The substrate surface was irradiated by the VUV for 10 minutes.

During the Step (2), the VUV chamber was evacuated to the order of 10^{-4} Pa to reduce the number of water molecules included in the chamber. Since the gas pressure created by using a turbo molecular pump was almost equivalent to that of water, the concentration of water molecules was calculated to be approximately 1.66×10^{-5} mmol/m^3 at the pressure of 10^{-4} Pa.

5.2.4. XPS surface analyses

The XPS surface analysis process was mentioned in chapter 4. For Pt, the analysis depths corresponding to take-off angles of 15° was 0.1 nm, as the inelastic mean free path (λ) in Pt was 0.4 nm [3].

5.2.5. Bonding process and strength evaluation method

The bonding processes for all three kinds of modification methods (i.e. vapor-assisted VUV, FAB, and simple VUV) were same as follows:

(1) The surface modified substrates were transported to a flip-chip bonding chamber (without exposure to atmosphere).

(2) PEEK and Pt substrates (with Pt on the bottom side) were contacted with the load of 1000 N, which was necessary to ensure intimate contact between a pair of the surfaces.

(3) The contacted substrates were heated to 150 °C, which was around the glass transition temperature of PEEK (143 °C) [4].

(4) The substrates were kept at 150 °C for 10 minutes.

After the bonding, a shear strength test (Nordson) was carried out to evaluate bonding strain energy

release rate between PEEK and Pt.　The shear speed was controlled at 50 μm/s and the maximum force just before the fracture was recorded.　In addition, the nominal bonding area was measured using Photoshop software (Adobe) during the bonding strength calculation.　A fracture observation was carried out by scanning electron microscope (SEM, NB5000, Hitachi).

5.3　**Results and discussions**

5.3.1. XPS analyses results

5.3.1.1 Vapor-assisted VUV modification effects

The XPS analyses confirmed the vapor-assisted VUV modification effects on PEEK as discussed in chapter 4.
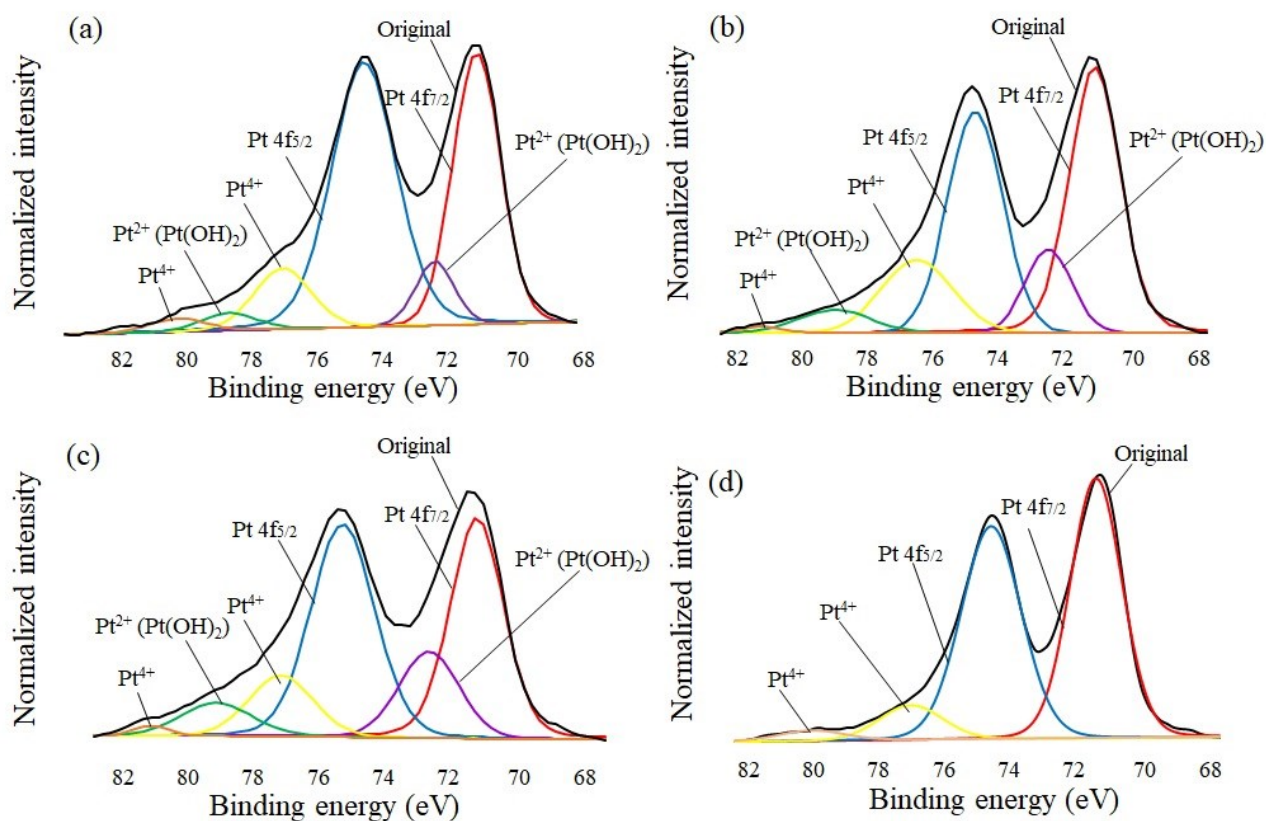

Fig. 5.1 Pt 4f curve fitting for the Pt surface modifications under the vapor concentration of (a) 36.0, (b) 165, (c) 656 mmol/m^3, and (d) untreated Pt surface

As for Pt, **Fig. 5.1(a), (b) and (c)** show results of Pt 4f spectra curve fitting for the vapor concentration conditions on 36.0, 165 and 656 mmol/m^3, respectively.   By comparison, a curve fitting result of unmodified Pt is shown in **Fig. 5.1(d)**.   **Fig. 5.1(d)** showed that the Pt 4f spectra of the unmodified Pt outmost surface (0.1 nm) could be deconvoluted into four peaks: Pt $4f_{7/2}$ and Pt $4f_{5/2}$ double peaks at 71.3 and 74.5 eV [5, 6] respectively, Pt^{4+} from Pt $4f_{7/2}$ at 76.6 eV [5, 6], and Pt^{4+} from Pt $4f_{5/2}$ at 80.4 eV [5, 6].   After the vapor-assisted VUV modifications, novel peaks with the energy gap of 1.3 ± 0.2 eV and 6.5 ± 0.6 eV apart from Pt $4f_{7/2}$ peaks occurred.   These positions matched with Pt^{2+} from Pt $4f_{7/2}$ and Pt $4f_{5/2}$, respectively.   Since the vapor-assisted VUV modification method contained sufficient ·OH radicals in chamber, these novel peaks were considered as Pt(OH)$_2$ peaks [5, 6].   Therefore, the vapor-assisted VUV method was confirmed effective on the Pt surface modification.

5.3.1.2 FAB and simple VUV modification effects

The modification effects of FAB and simple VUV were evaluated by XPS.   Since an H element peak was covered with other peaks, it was difficult to be evaluated [7].   So we focused on atomic concentration ratio of O to C (i.e. O/C ratio).   Before the surface modifications, the O/C ratio of the outmost PEEK surface (0.9 nm) was about 0.22, while the ideal PEEK structure ((-O-C$_6$H$_4$-O-C$_6$H$_4$-C(=O)-C$_6$H$_4$-)$_n$) was about 0.16.   After the FAB and the simple VUV modifications, the O/C ratio of the outmost surface changed to 0.02 and 0.98, respectively.   It was considered that the excess amount of O on the initial surface came from the organic contamination, which would be removed via the modifications.   Moreover, rapid atomic concentration decrease of O indicated condensation of C during the FAB modification, and thus a low molecular weight oxide material film was formed on the outmost surface [8, 9].   The increment of the O content after the simple VUV modification was considered attributable to the water molecules from inside the chamber.   A similar tendency was observed in the atomic concentration of O and C on the Pt substrate.
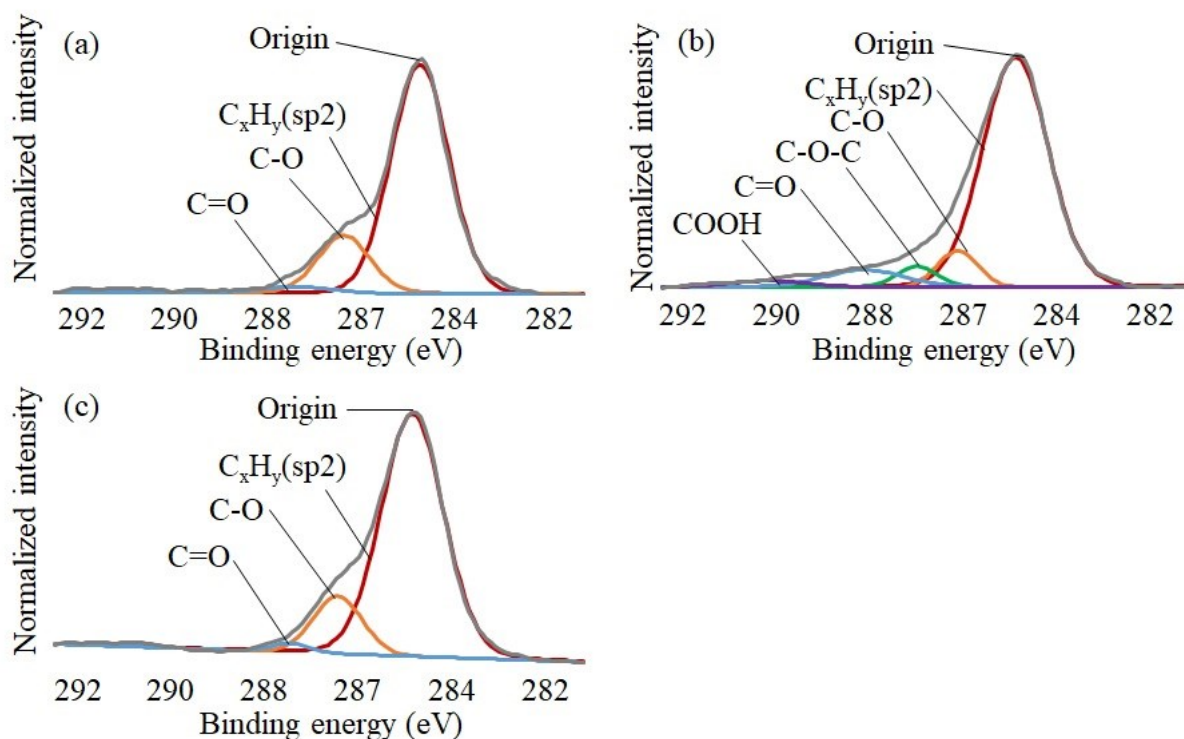
Fig. 5.2 C 1s spectra curve fitting of PEEK (a) before modification and (b) after the FAB modification, and (c) after the simple VUV modification.
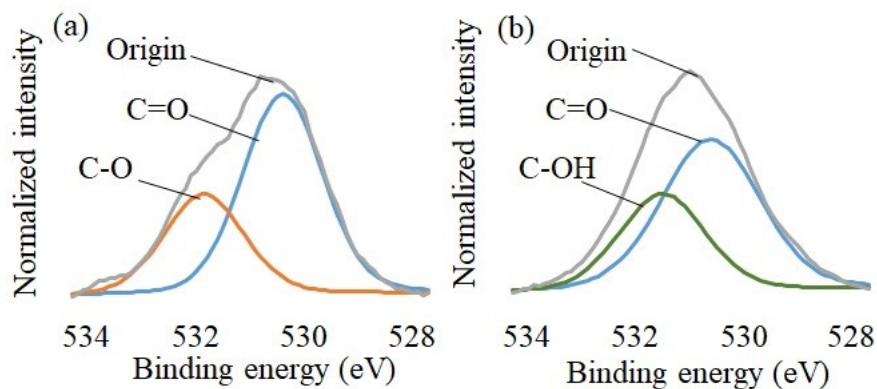
Fig. 5.3 O 1s spectra curve fitting of PEEK (a) before and (b) after the simple VUV modification

Fig. 5.2(a) shows the deconvoluted C 1s spectra of unmodified PEEK, while **Fig. 5.2(b) and (c)** respectively show those after the FAB and the simple VUV modification.　In **Fig. 5.2(a) and (c)**, three peaks could be deconvoluted from the original peak, in which the highest could be identified as a C_xH_y peak [7, 10, 12, 13], and the other two peaks with energy gaps of about 1.7 eV and 2.8 eV matched with

a C-O peak and C=O peak [7, 10, 12, 13], respectively.   In **Fig. 5.2(b)**, the original peak had a different

curve from those in **Fig. 5.2(a) and (c)**, which was considered to be due to the C condensation on the

outmost surface of PEEK during the FAB modification.   The original peak was considered to be

deconvoluted into 5 peaks: a C_xH_y peak, a C-O peak, a C-O-C peak, a C=O peak, and a COOH peak [7,

10-12].   **Fig. 5.3** shows the O 1s spectrum of PEEK before and after the simple VUV modification.   In

Fig. 5.3(a), the original peak could be deconvoluted into two peaks with the energy gap of about 1.5 eV,

and thus they were identified as a C=O peak and a C-O peak [7, 10-12], respectively.   In **Fig. 5.3(b)**,

the deconvoluted two peaks were closer than those in **Fig. 5.3(a)**, and the energy gap was about 0.9 eV,

which was believed to be a C=O peak and a C-OH peak [7, 10-12], respectively.   Therefore, the outmost

structure of PEEK was conceivable to include C-OH groups after the simple VUV modification.   The
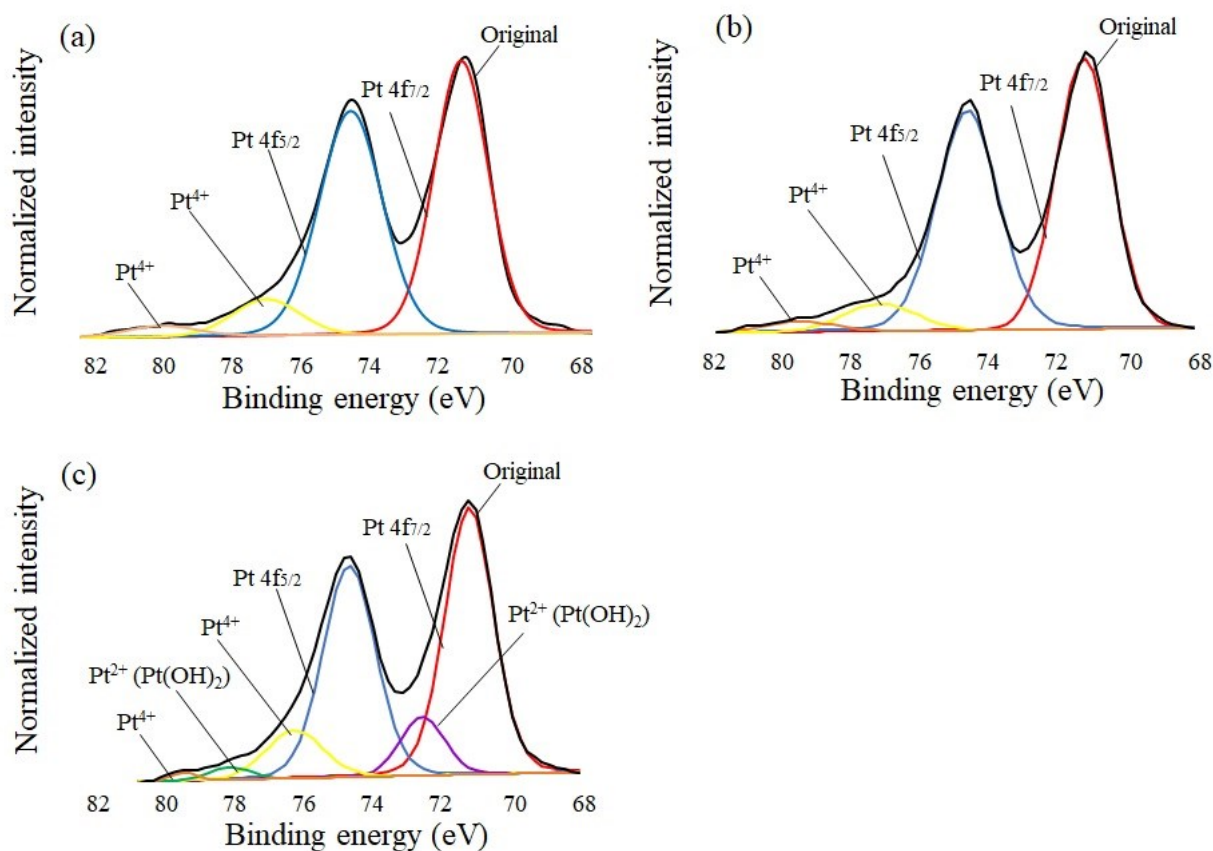

Fig. 5.4 Pt 4f spectra curve fitting of (a) unmodified Pt, (b) FAB modified Pt, and (c) simple VUV
modified Pt

O 1s spectra after the FAB modification was too weak and contained too much noise, which could not be fitted well, thus the spectra was not used in this thesis. **Fig. 5.4(a), (b) and (c)** were the spectra of Pt 4f before and after FAB and simple VUV modifications, respectively. In **Fig. 5.4(a) and (b)**, the original peaks had similar curves, which could be deconvoluted from four peaks: Pt $4f_{7/2}$, Pt $4f_{5/2}$ and Pt^{4+} from Pt $4f_{7/2}$ and Pt $4f_{5/2}$, respectively. In **Fig. 5.4(c)**, the original peak curve was different from those in **Fig. 5.4(a) and (b)**, in which two new peaks at approximately 1.4 eV and 6.6 eV higher than the Pt $4f_{7/2}$ peak were deconvoluted. In consideration of this energy gap and the presence of water molecules in the chamber, this deconvoluted peak corresponded to the peaks of $Pt(OH)_2$ [11].

From these results, it could be concluded that the FAB modification was effective on surface cleaning, while the simple VUV modification was capable of creating hydrate bridge layers on both PEEK and Pt surfaces.

5.3.2 Bonding strength and theoretical calculation

5.3.2.1.Bonding strength results

Shear strengths for each condition was summarized in **Table 5.2**. From the strengths, it could be known that surfaces modified at the vapor concentration of 36.0 mmol/m³ had higher strength than ones modified at 656 mmol/m³. It was in good agreement with the surface modification effects evaluated by the O/C ratio as discussed in chapter 4 in which excessive humidity limited the modification effects. Furthermore, both vapor-assisted VUV modified samples showed higher strength than the FAB modified ones. This was considered that after the FAB modification, there was not sufficient chemical functional groups for the diverse substrates to react instead of effect on surface cleaning. The vapor-assisted VUV modified samples showed strengths at same level as the simple VUV modified ones because the mechanisms of these surface modifications were approximately same in modifying substrate surfaces with radicals dissociated by VUV. However, with better controlled humidity, the modification effect

Table 5.2 Shear strengths and strain release energy rates of the vapor-assisted VUV, FAB, and simple VUV modified PEEK-Pt bondings

Method	Sample No.	Bonding strength	Strain energy release rate
Vapor-assisted VUV (36.0 mmol/m³)	1	0.12 MPa	5.0×10^{-3} N/m
	2	0.99 MPa	3.4×10^{-1} N/m
	3	1.15 MPa	4.6×10^{-1} N/m
	Average	0.75 MPa	2.0×10^{-1} N/m
Vapor-assisted VUV (656 mmol/m³)	1	0.15 MPa	7.9×10^{-3} N/m
	2	0.21 MPa	1.5×10^{-2} N/m
	3	0.26 MPa	2.4×10^{-2} N/m
	Average	0.21 MPa	1.5×10^{-2} N/m
FAB	1	0.03 MPa	3.2×10^{-4} N/m
	2	0.04 MPa	5.6×10^{-4} N/m
	3	0.18 MPa	1.1×10^{-2} N/m
	Average	0.09 MPa	2.8×10^{-3} N/m
Simple VUV	1	0.45 MPa	7.1×10^{-2} N/m
	2	0.10 MPa	3.5×10^{-3} N/m
	3	0.08 MPa	2.2×10^{-3} N/m
	Average	0.21 MPa	1.5×10^{-2} N/m

could be optimized, and thus the samples modified with the vapor-assisted VUV under the vapor concentration condition of 36.0 mmol/m³ had a higher strength than the simple VUV modified ones. Therefore, it could be concluded that the purposed vapor-assisted VUV modification could compete with the conventional methods using high vacuum condition.

5.3.2.2. Theoretical strain energy release rate

Since the PEEK-Pt bonding used diverse materials, the interface strain energy release rates calculations were adjusted from those equations discussed in chapter 2 as follows:

$$G_{nominal} = \frac{\sigma^2}{4}\left(\frac{L_{PEEK}}{E_{PEEK}} + \frac{L_{Pt}}{E_{Pt}}\right) \tag{5.27}$$

$$G_{nominal} = \Omega G_{real} \tag{5.28}$$

where the E_{PEEK}, E_{Pt}, L_{PEEK}, and L_{Pt} represented young's modulus and thickness of PEEK and Pt, respectively. The results were also summarized in **Table 5.2**. The strain release energy rate of the

vapor-assisted VUV could reach 2.0×10^{-1} N/m. As a comparison, the surface free energy of PEEK was 4.2×10^{-2} N/m. Hence, the strain release energy of the samples modified with the vapor-assisted VUV reached limit of the theoretical energy in PEEK. Although the calculated value became higher than the true value due to some assumptions which ignored energy consumed by plasticity and anchoring effect, it could be considered that the strain release energy of the PEEK-Pt interface was as high as a PEEK bulk. Therefore, it could be concluded that our PEEK-Pt bonding by the vapor-assisted VUV modification was successful.

5.4. Conclusions

This chapter described the results on PEEK-Pt hybrid bonding at 150 °C through vapor-assisted VUV. Similar to previous chapters, the calculated strain release energy reached 2.0×10^{-1} N/m (0.75 MPa) at low vapor molecule concentration (36.0 mmol/m^3), which was comparable with PEEK theoretical limit energy of 4.2×10^{-2} N/m, while a high concentration (656 mmol/m^3) condition showed smaller value than this. Contrary to this, the samples obtained by conventional FAB in high vacuum and simple VUV irradiation showed the values of 0.088 and 0.21 MPa, respectively. From the results presented above, we could conclude that the VUV-induced bridge formation was highly effective to create direct hybrid interfaces among polymers and metals, at low temperatures without vacuum.

The proposed vapor-assisted VUV modification achieved the world first direct bonding between polymer and metal at such low temperature. The vapor-assisted VUV technology provided a strong candidate for future polymer-metal hybrid bonding, and was expected to be used in bio-MEMS applications.

Refences

[1] W. Fu, A. Shigetou, S. Shoji, J. Mizuno, J.Mater. Sci. Eng. B,, 7 (2017) 49.

[2] W. Fu, A. Shigetou, S. Shoji, J. Mizuno, Mater. Sci. Eng. C, 79 (2017) 860.

[3] C. J. Powell, NIST Electron Inelastic-Mean-Free-Path Database, ver. 1.2., 2010.

[4] D. Shukla, Y. S. Negi, J. S. Uppadhyaya, V. Kumar, Polym. Rev. 52 (2012) 189.

[5] J. F. Moulder, W. F. Stickle, P. E. Sobol, K. D. Bomben, "Handbook of X-ray Photoelectron Spectroscopy" (Physical Electronics, Eden Prairie, MN,1992) P. 180

[6] N. R. Mathe, M. R. Scriba, N. J. Coville, Int. J. Hydrogen Energy, 39 (2014) 18871.

[7] H.W. Tien, Y. L. Huang, S. Y. Yang, J. Y. Wang, C. C. M. Ma, Carbon, 49 (2011) 1550.

[8] W.J. van Ooij, R.H.G. Brinkhuis, Surf. Interface Anal. 11 (1988) 430.

[9] S.O. Saied, J.L. Sullivan, T.C. houdhury, C.G. Pearce, Vacuum 38 (1988) 917.

[10] G.P. Lopez, D. G. Castner, R. D. Ratner, Surf. Interface Anal., 17 (1991) 267.

[11] J. F. Moulder, W. F. Stickle, P. E. Sobol, K. D. Bomben, "Handbook of X-ray Photoelectron Spectroscopy" (Physical Electronics, Eden Prairie, MN,1992) P. 40.

[12] H. Shinohara, J. Mizuno, S. Shoji, Sens. Actuators A, 165 (2011) 124.

[13] J. F. Moulder, W. F. Stickle, P. E. Sobol, K. D. Bomben, "Handbook of X-ray Photoelectron Spectroscopy" (Physical Electronics, Eden Prairie, MN,1992) P. 44.

Chapter 6

<u>Conclusion</u>

In this thesis, the direct hybrid bonding methods for polymers and metals, which could be carried out at low temperature without vacuum atmosphere, were developed by utilizing the VUV-induced surface activation with ultrathin bridge layers formation.   Such technology would be of a practical use in realizing robust and flexible biomedical micro electromechanical systems (bio-MEMS) packaging. Given poly-ether ether ketone (PEEK), poly-oxymethylene (POM), poly-methyl methacrylate (PMMA) and Pt as the typical starting materials, we proposed to use the dissociated water molecules and self-assembled monolayer (SAM) during/after the vacuum ultraviolet (VUV) irradiation to form the bridge layers, according to the operating and glass transition temperature of organic materials.   The evolution of chemical binding condition on each material and the bond mechanisms were investigated to optimize the process parameters, then the interfacial structure was analyzed.   The theoretical calculations on bonding strength was also carried out to evaluate the bondability.   Results showed that the direct hybrid bonding was found feasible with the bonding energy as high as surface free energy of bulk material. These achievements are elaborated on in Chapter 1 ~ 5 is as follows:

Chapter 1 provided the concept of a direct hybrid bonding among polymers and metals, and the necessary technologies for sufficient bondability on the different materials at the same time without using high temperature and vacuum.   Since the bio-MEMS packages and artificial organic parts required a thin, chemically and thermally robust, and flexible integration technology, we had to develop a low temperature direct bonding technology.   In addition, vacuum atmosphere had to be eliminated for the sake of adoptability to conventional industrial lines.   Therefore, we proposed to use the VUV irradiation

in nitrogen atmosphere for the initial surface activation.   For the organic material with low operating and glass transition temperature, POM and PMMA (less than 100 °C) for example, we chose to create ultrathin SAM layers to utilize epoxy and amine groups as the bridge.   For the heat-tolerant and inorganic materials like PEEK and Pt, respectively, the vapor-assisted bridge formation was adopted.

In Chapter 2, a POM direct bonding was achieved at 100 °C through the use of (3-aminopropyl)triethoxysilane (APTES) and (3-glycidyloxypropyl)trimethoxysilane (GOPTS) monolayers.   It was the first report of a POM direct bonding at such low temperature.   By using such method, the required bonding temperature could be reduced, and polymers with poor heat resistance could be applied in bondings that conventionally required high process temperature.   Furthermore, it had to be noticed that SAM modifications could also be applied on metals.   Therefore, the proposed SAM modification method could also provide candidates for polymer-metal hybrid bondings.

In Chapter 3, a POM-PMMA bonding was realized at room temperature through the use of APTES monolayer.   It was the first report that bio-inert polymers could be bonded at room temperature.   The proposed method provided a strong alternative bonding technology for biomedical applications, especially those who had to avoid scald such as dental therapies.

Chapter 4 elaborated a novel vapor-assisted VUV modification method.   The established vapor-assisted VUV method was confirmed to be highly compatible that it could modify polymers as well as metals simultaneously.   Its polymer modification effect was controlled by humidity (i.e. vapor concentration), and the modification effect could be optimized.   Since its compatibility, the proposed vapor-assisted VUV could help bond polymer-polymer, metal-metal, and polymer-metal interfaces simultaneously, which was of practical interests in the industrial fabrications.

In Chapter 5, a PEEK-Pt hybrid bonding was realized at 150 °C through the vapor-assisted VUV surface modification.   It was the first report of the polymer-metal hybrid realized at such low temperature.   By utilizing the proposed vapor-assisted VUV technology, the complex wiring metal

packaging in implantable bio-MEMS became feasible because all the three interfaces could be bonded without voids. In addition, except from bio-MEMS packaging, the proposed vapor-assisted VUV could also be applied in industries that required lightweight structure, such as automobile, because its atmospheric low temperature process had high compatibility with conventional processes and provided a possibility for large-area modification.

This doctoral thesis confirmed that polymers with low surface free energies could be applied in direct bondings through suitable surface modifications. These modification methods greatly contributed to the widespread of polymer-based applications including biomedical devices, automobiles and aircrafts.

Future work on heterogeneous bonding of polymer-metal will include practical realization of metal wire embedded polymer direct bondings for bio-MEMS applications, which also involves physical morphology control of material surfaces. The investigation of this thesis was indispensable for future commercialization of biocompatible devices for life science and human health care.

List of achievement

\<Referred Journal Papers>

1. ○ **Weixin Fu**, Bo Ma, Hiroyuki Kuwae, Shuichi Shoji, and Jun Mizuno, "Low-temperature polyoxymethylene direct bonding via self-assembled monolayer", Japanese Journal of Applied Physics, Vol. 57, 02BB01, 2018.

2. ○**Weixin Fu**, Akitsu Shigetou, Shuichi Shoji, and Jun Mizuno, "Low Temperature Direct Bonding between PEEK (Polyetheretherketone) and Pt via Vapor-Assisted Vacuum Ultraviolet Surface Modification", Journals of Materials Science and Engineering B, Vol. 7, No. 3-4, p. 49-62, 2017.

3. ○ **Weixin Fu**, Akitsu Shigetou, Shuichi Shoji, and Jun Mizuno, "Low-temperature direct heterogeneous bonding of poly ether ether ketone and platinum", Materials Science and Engineering C, Vol. 79, p. 860-865, 2017.

4. Takeshi Komino, Hiroyuki Kuwae, Akiko Okada, **Weixin Fu**, Jun Mizuno, Jean Charles Ribierre, Yuji Oki, and Chihaya Adachi, "In-Plane Anisotropic Molecular Orientation of Pentafluorene and Its Application to Linearly Polarized Electroluminescence", ACS Applied Materials and Interfaces, Vol. 9(32), p. 27054-27061, 2017.

5. **Weixin Fu**, Masatsugu Nimura, Takashi Kasahara, Hayata Mimatsu, Akiko Okada, Shuichi Shoji, Shugo Ishizuka, and Jun Mizuno, "A Metal Bump Bonding Method Using Ag Nanoparticles as Intermediate Layer", Journal of Electronic Materials, Vol. 44, No. 11, p. 4646-4652, 2015.

\<Referred International Conferences>

1. **Weixin Fu**, Bo Ma, Hiroyuki Kuwae, Shuichi Shoji, and Jun Mizuno, "A study on low temperature SAM modified POM direct bonding affected by VUV/O$_3$ irradiation", 5th IEEE international

workshop on low temperature bonding for 3D integration (LTB-3D), p. 211, May, 2017.

2. **Weixin Fu**, Akitsu Shigetou, Shuichi Shoji, and Jun Mizuno, "Low Temperature Bonding Between Polyether Ether Ketone (PEEK) and Pt Through Vapor-Assisted VUV Surface Modification", Research and Education Consortium for Innovation of Advanced Integrated Science International Symposium 2017 (CIAiS 2017), February, 2017.

3. **Weixin Fu**, Hiroyuki Kuwae, Bo Ma, Shuichi Shoji, and Jun Mizuno, "Low Temperature Direct Bonding of Polyoxymethylene (POM) through Self Assembly Monolayer (SAM)", International conference on electronics packaging (ICEP), p. 167-170, April, 2017.

4. **Weixin Fu**, Akitsu Shigetou, Shuichi Shoji, and Jun Mizuno, "Low temperature bonding between polyether ether ketone (PEEK) and Pt through vapor assisted VUV surface modification", IEEE 66th Electronic Components and Technology Conference (ECTC), p. 2541-2546, May, 2016.

5. Bo Ma, Hiroyuki Kuwae, Akiko Okada, **Weixin Fu**, Shuichi Shoji, and Jun Mizuno, "VUV/O_3 assisted single crystal quartz bonding with amorphous SiO2 intermedicate layer for manufacturing optical low pass filter", International conference on electronics packaging (ICEP), p. 447-450, April, 2016.

6. **Weixin Fu**, Akitsu Shigetou, Shuichi Shoji, and Jun Mizuno, "Low temperature direct bonding of PEEK and Pt through VUV/FAB surface treatment", International conference on electronics packaging (ICEP), p. 302-305, April, 2016.

7. Bo Ma, Hiroyuki Kuwae, Akiko Okada, **Weixin Fu**, Shuichi Shoji, and Jun Mizuno, "Low temperature direct bonding of single crystal quartz substrates for high performance optical low pass filter using amorphous SiO2 intermediate layers", IEEE International conference on micro electro mechanical systems (MEMS), p. 25-28, 2016.

8. **Weixin Fu**, Akitsu Shigetou, Shuichi Shoji, and Jun Mizuno, "Low Temperature Direct Bonding of Polyether Ether Ketone (PEEK) and Pt", 10th international microsystems, packaging, assembly and

circuits technology conference (IMPACT), p. 217-220, October, 2015. (Best student paper award)

9. **Weixin Fu**, Jun Mizuno, Takashi Kasahara, Akiko Okada, Hiroshi Nishikawa, Akitsu Shigetou, and Shuichi Shoji, "Low temperature bump bonding realized by single-micrometer Ag-nanoparticle bumps", The 5th International Symposium on Advanced Materials Development and Integration of Novel Structured Metallic and Inorganic Materials (AMDI-5) Conjunction with 6th IBB Frontier Symposium, November, 2014.

10. **Weixin Fu**, Takashi Kasahara, Akiko Okada, Shuichi Shoji, Akitsu Shigetou, and Jun Mizuno, "Low temperature and low pressure bump bonding realized by single-micrometer Ag-nanoparticle bumps", 4th IEEE international workshop on low temperature bonding for 3D integration (LTB-3D), p. 47, June, 2014.

11. **Weixin Fu**, Takashi Kasahara, Akiko Okada, Jun Mizuno and Shuichi Shoji, "Novel Bump Bonding method using Ag nanoparticle coated Cu bump through squeegee-coatig", The 5th NIMS/MANA-Waseda Univesity International Symposium, March, 2014.

12. **Weixin Fu**, Jun Mizuno, Shuichi Shoji, Takashi Kasahara, Akiko Okada, and Shugo Ishizuka, "Novel Bonding Method Using Cu Bumps Coated With Flexible Ag Nanoparticle Layer Formed By Squeegee-Coating", IEEE CPMT symposium Japan (ICSJ), p. 1-4, November, 2013. (Young award)